MCRWPT Design Through Analog Filter Theory

by

Aleksander Jack

Submitted in partial fulfillment of the requirements
for the degree of Master of Applied Science

at

Dalhousie University
Halifax, Nova Scotia
August 2020

Table of Contents

List of Tables

List of Figures

Abstract

Magnetically-Coupled Resonant Wireless Power Transfer (MCRWPT) is an emerging technology and the subject of extensive research. Existing research is primarily focused on improving the magnetic coupling properties of the four coils. The circuit parameters of these coils have been of less focus. These parameters are generally determined using optimization routines in an attempt to elicit the desired MCRWPT system performance.

While this has proven to be an acceptable method of designing MCRWPT systems, it would make more sense to determine the desired performance of the systems, and then directly choose circuit parameters which will meet these requirements. Filter theory is chosen to realize this desire since the filter design has been optimized and standardized.

This thesis begins by illustrating how filter theory techniques can be applied to the efficiency of an MCRWPT system. The square of the mutual coupling between the two resonator coils is chosen to act as the input variable which controls the power transfer efficiency of the entire system. This allows for MCRWPT systems to be specifically designed to maintain a high efficiency between two user-chosen coil separations.

Next, the equations to map the MCRWPT efficiency equation to the filter transfer function is presented. They allow for a high transfer efficiency to be realized across a wide range of separations with the application of the filter theory. The transmitted power is found to be maximized at a certain separation and decrease when the coils are moved away from this separation.

Finally, a modified solution or mapping equation is presented. This solution maintains a high transfer efficiency beyond the range specified by the filter used to design the system. Unlike the original mapping, it also maintains a high transmitted power level over a wide range of coil separations.

List of Abbreviations Used

WPT	Wireless Power Transfer
MCR	Magnetically-Coupled Resonant
PTE	Power Transfer Efficiency

Acknowledgements

I want to extend my sincerest appreciation to Dr. Zhizhang (David) Chen, who has supervised my work, answered my questions, and directed my focus over the past two years. I would have been unable to progress this far without his assistance.

I would also like to thank my committee members Dr. Colin O'Flynn and Dr. Guy Kember for agreeing to participate and help in my defense.

Special thanks also go out to Nicole Smith, Tamara Cantrill, and the rest of the faculty, staff, and graduate students in the ECED Department who have not only helped me through this degree but through my undergraduate experience as well.

Finally, I would like to thank my family for their support these past two years, and for putting up with me for the past five months during which I worked from home.

Chapter 1 Introduction

1.1 Background

As technology progresses, the electronics sector continues to grow. Estimations for the number of IoT connected devices in use by 2025 range from 41.6 billion [1] to 75.44 billion [2]. Due to the nature of electronic devices, all of these systems will require some external source of electrical power. This source can take many different forms. For some devices such as kitchen appliances, this can easily be accomplished using a traditional power cord. However, many other devices such as smart watches or cell phones cannot be powered by these means as they have an inherent need to be mobile and untethered. Current solutions to this issue generally involve limiting the mobility of these devices for a short period in order to recharge an onboard battery. This solution is functional, but not ideal.

Inspiration for a possible solution to this issue can be found in the communication methods employed in consumer electronics. Currently, a common trend throughout the industry has been to remove physical data connections wherever possible. Many computer manufacturers have stopped including ethernet ports in their laptops, and the latest flagship cellphone models from both Apple and Samsung do not include 3.5mm audio connections. Instead of physical connections, users rely on wireless communications methods such as Wi-Fi or Bluetooth to keep their devices connected to other devices or the outside world in general.

Given the desire to power electronic devices without limiting their mobility, and the flexibility and mobility observed in the wireless communications field, the concept of wireless power transfer (WPT) seems attractive. WPT been applied to a wide range of consumer products

ranging from toothbrushes to cellphones. Unfortunately, there are limits to these techniques. While communications techniques such as Wi-Fi have been developed to the point where a user may use these systems over a wide range of distances and device orientations relative to the transmitter without loss of performance, WPT technology does not enjoy these same advantages. Currently, devices charged wireless generally use inductive coupling to transmit energy. While this provides a reasonable power transfer efficiency (PTE), the efficiency cannot be maintained for large separations or all device orientations [3].

In 2007, researchers at MIT developed a new technique for WPT known as "Magnetically-Coupled Resonant Wireless Power Transfer" (MCRWPT). This technique uses a pair of resonant coils to improve the PTE at longer ranges in comparison to traditional inductive coupling [4]. Researchers have identified several potential applications for this technology, ranging from electric vehicles [5], to implanted medical devices [6], to mobile sensor systems located in the field [7].

Currently, many of the design techniques developed so focus on different methods of designing physical coils to improve transmission efficiencies such as auxiliary strips [8], impedance conversion [9], or electromagnetic characteristics [10]. These methodologies attempt to optimize the physical characteristics of their coils to improve the magnetic coupling between the transmitter and the receiver. This largely results in complex optimization schemes that are time- and resource-intensive and quite complex. The development of a simpler method to design MCRWPT systems appears to be desirable.

In contrast to MCRWPT technology, analog filter theory is a much older and more mature field, with several patents and papers on the subject dating back to the first three decades of the twentieth century [11, 12, 13]. Evidence of the long term knowledge and understanding in this subject is highlighted by the fact that both simple and complex analog filters are a common topic in many undergraduate programs.

From a circuitry perspective, analog filters and MCRWPT systems are quite similar. Both systems are made up of a combination of resistors, inductors, and capacitors. Both systems also show frequency-selective characteristics which can be manipulated by changing the values of their electronic components.

Given these similarities between the concepts of filter transfer functions and power transfer efficiency, it should be possible to graft some components of filter theory into WPT theory. If this were to be done, the resulting system would possess the existing optimization of the filter. This grafting and the resulting MCRWPT designs will be the focus of this thesis.

1.2 Research Goals

There are two primary goals for this thesis. First, this research aims to prove that filter theory can be successfully grafted into MCRWPT theory. Second, a viable general solution that implements a filter design in an MCRWPT system is to be presented to illustrate the capabilities of such a design process.

1.3 Contributions

This thesis contributes three concepts or techniques to state of the art:

1. Filter theory is shown to be compatible with the MCRWPT theory. This allows for the design of MCRWPT systems using well known and understood techniques from filter theory.
2. A rigorously derived general solution or mapping that implements a filter transfer function in describing an MCRWPT system is presented. This solution is capable of meeting all of the specified filter parameters. The solution is also capable of having its filter or coil parameters altered without endangering the viability of the found solution.
3. A modified solution or mapping equation is also presented. This solution exceeds the input filter parameters and is capable of maintaining maximum received power over a wide range of coil impedance parameters. This feature is desirable, but not possible using the original general solution.

1.4 Thesis Organization

This thesis is organized into six sections, along with the abstract and reference list. The contents of each section are described below:

- Section one describes the background for this thesis and lays out the various goals and contributions of the work described in this document.
- Section two reviews the existing theory for WPT systems with an emphasis on MCRWPT systems. Current design methodologies for these systems are also considered.
- Section three is concerned with the mathematical derivation of an MCRWPT system and the process of grafting a filter transfer function into this system. It also considers what the

WPT analog of a filter's input frequency should be and presents the bridging equations which can be solved to obtain the general solutions.

- Section four begins by presenting a solution to the bridging or mapping functions which implements a filter transfer function in an MCRWPT system. It also discusses some of the limitations to this process, the process to be used to convert a general solution into a set of impedances, and alternate solutions to these equations.
- Section five takes the solutions derived in section four and simulates them in Matlab and ADS. Various characteristics of these solutions are considered and examined.
- Section six summarizes the work described in this document and presents several recommendations on future research to be conducted.

Chapter 2 Overview of Existing Theory and Design

This section will review WPT in general, followed by a more in-depth consideration of MCRWPT. Following this, current research in the field will be examined, and the overall trends will be discussed.

2.1 Wireless Power Transfer Theory

Commercially, wireless power transfer may be thought of as relatively new technology. In a scientific sense, however, wireless power transfer has a long history. In the early 1900s, Nikola Tesla conducted several experiments in this field [14]. In the 1960s, WPT was attempted using microwave beamforming and a rectifying antenna [15]. These tests were successful in transmitting 4W of power with a PTE of 50%. This technique was capable of transmitting power over a range of several kilometers [16]; however, it was of limited use due to the line-of-sight requirement [8]. Modern techniques for wireless power transfer are focused on shorter transmission ranges and generally use either inductive coupling or MCRWPT.

Inductive coupling systems are accomplished using transmitting and receiving coils, as shown in Figure 2.1.1. A time-varying current is generated in the driver coil, which in turn generates a magnetic field. This magnetic field then interacts with the load coil to generate a voltage and current which can be used to power the load. This technology is the basis for the Qi wireless charging standard [17].

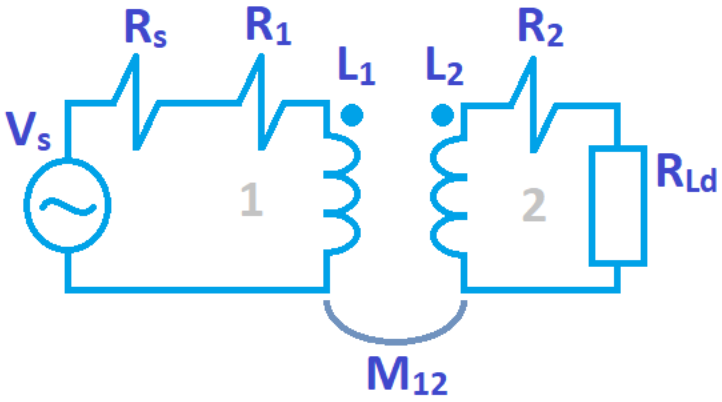

Figure 2.1.1: The Circuit Diagram for an Inductively Coupled Wireless Power Transfer System

While inductively coupled systems are relatively simple and capable of reasonable efficiency, they are limited in their transmission range. As the coil separation is increased, the maximum transfer efficiency drops on the order of $\frac{1}{d^3}$ [3] where d is the distance between the transmitting and receiving coils.

Magnetically-coupled resonance wireless power transfer is a more modern technique which was developed by MIT researchers in 2007. Unlike inductively coupled systems, a magnetically-coupled resonant system consists of four coils: one driver coil, one load coil, and two resonant coils. The driver coil and one of the resonator coils are located within the transmitting device, and the other resonator coil and the load coil are located within the receiving device [4]. A circuit diagram for this system is shown in Figure 2.1.2, and the physical implementation of this system is shown in Figure 2.1.3.

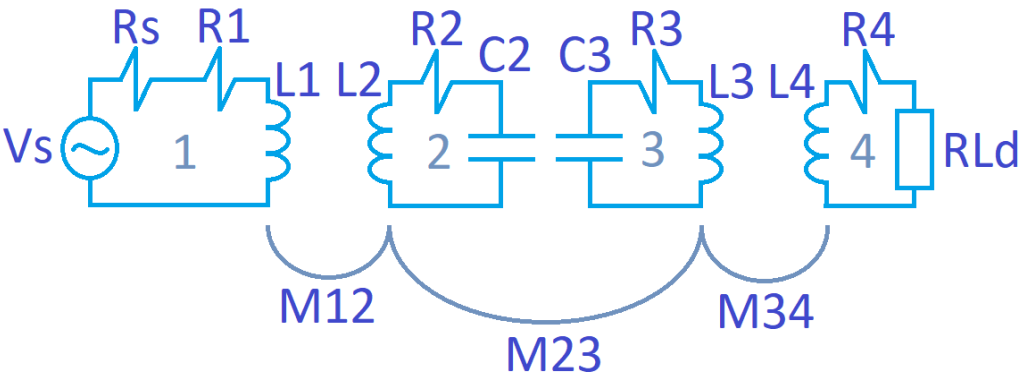

Figure 2.1.2: The Circuit Diagram for a basic MCRWPT System

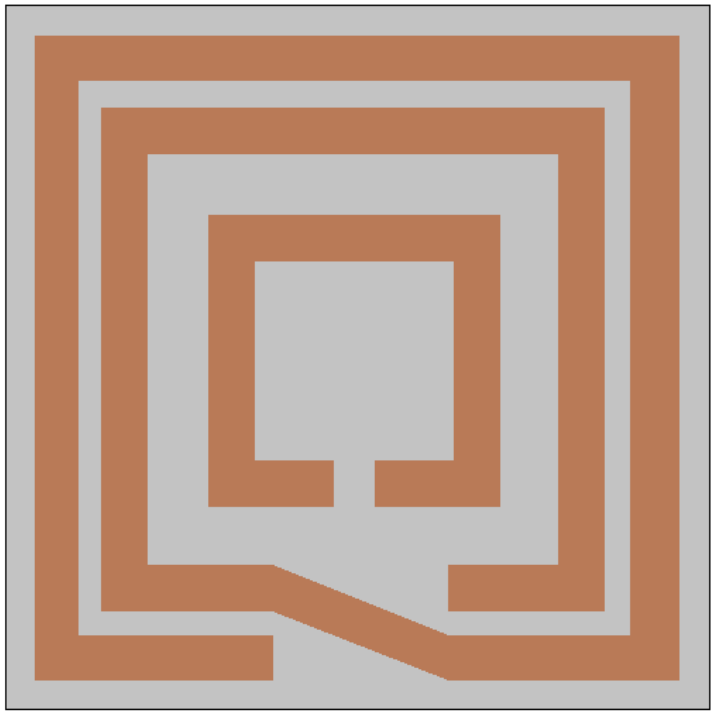

Figure 2.1.3: A Physical Implementation of an MCRWPT System

An MCRWPT system has three distinct coupling states: Over-coupled, critically coupled, and under-coupled. The coupling state of any given system is a function of that system's electrical characteristics, its operating frequency, and the separation distance between the transmitting and receiving coils. In most systems, the only variable which may be altered is the separation distance; however, some systems have been proposed which rely on multiple operating

frequencies [18] or variable electrical parameters [19] to manipulate the coupling state of the MCRWPT system.

A system is said to be over-coupled when the distance between the transmitting and receiving coils is less than an ideal value. In this region, the large coupling between the transmitting and receiving coils causes a frequency-splitting phenomenon, which in turn reduces the transmission frequency [8].

If the distance transmitting and receiving coils were to be increased until the frequency-splitting phenomenon disappears, an MCRWPT system is considered to be critically-coupled. This coil separation is ideal, and the system will operate at the maximum possible efficiency while this separation is maintained.

In the case that the coil separation of an MCRWPT system is increased beyond the ideal distance, the system will become under-coupled. In this configuration, there is insufficient coupling to allow for a high PTE to exist.

In addition to the limitations imposed by coil separation, coil orientation is also a consideration in an MCRWPT system. Generally speaking, the coils used in an MCRWPT system exhibit the maximum coupling when they are properly aligned, as shown in Figure 2.1.4. If the alignment of a pair of coils is disturbed, for example, by a small rotation of one of the coils around the vertical axis, the magnetic coupling observed will decrease, and the state of the MCRWPT system will

be changed [20]. This presents issues for mobile systems when proper coil alignment is not guaranteed.

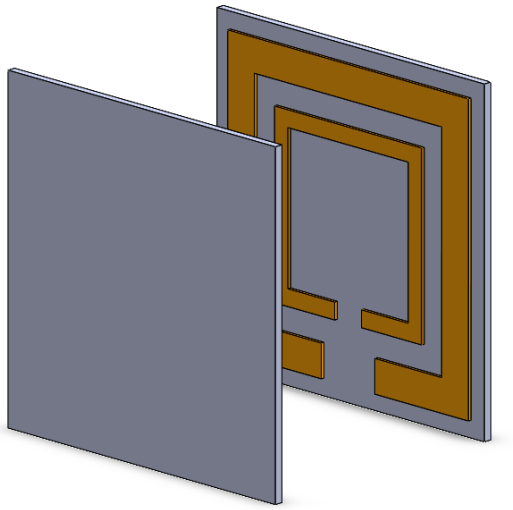

Figure 2.1.4: Two Properly Aligned Coils

Figure 2.1.5 shows a plot of the power transfer efficiency and received power as a function of coil separation in a typical system, as described in [8]. It can be seen that high efficiency can only be maintained over a short range of coil separations.

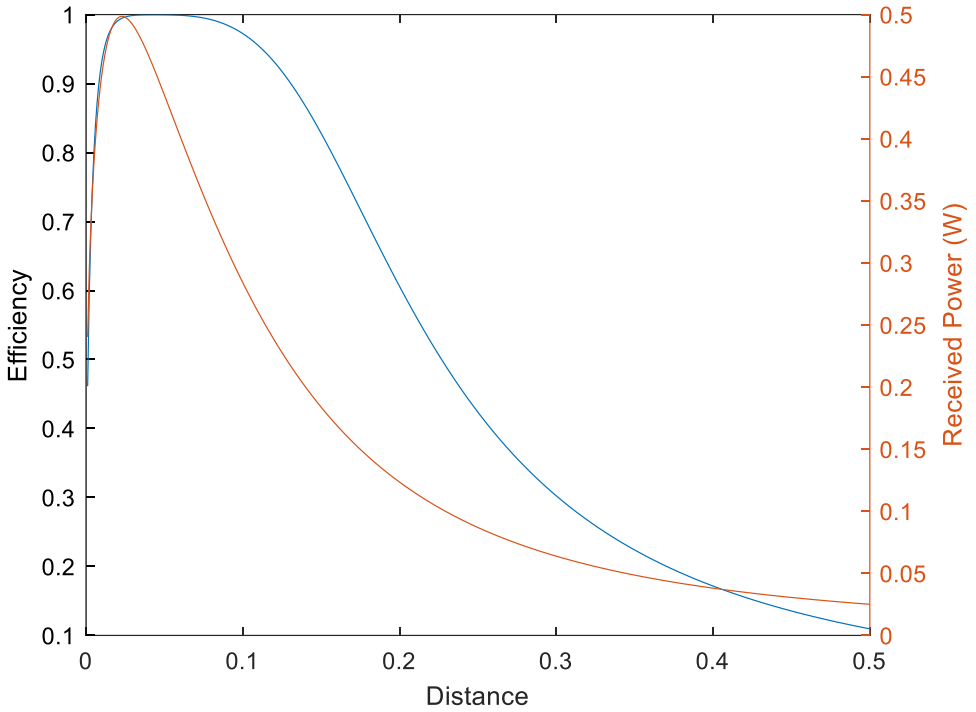

Figure 2.1.5: The Power Transfer Efficiency and Received Power as a Function of Distance

2.2 Current Research in MCRWPT

The range of potential technologies that could be powered by MCRWPT is extensive. Some examples of this range are as follows:

1. Cellphones, Smart Watches, and other Personal Electronic Devices. As previously mentioned, the latest flagship cellphones from both Apple and Samsung can be powered wirelessly using the Qi standard. MCRWPT technology could allow for these devices to be charged in the pockets of their users instead of having to place the devices on a stand or docking platform.
2. Implantable Medical Devices. A wide variety of research is being conducted to implement MCRWPT technology into implantable medical devices. Research ranges from detailed work considering the limitations of transmitting energy through the human

body [6, 8] to general system designs for an implementation which could be applied to these devices [21, 22]

3. Transportation. As electric vehicles increase in popularity, additional infrastructure must be developed to support them. While some of this research has been focused on powering stationary vehicles [3], other work has considered the possibility of powering vehicles while they are in motion as well [23, 24]. The technology has also been considered for use in Maglev trains [25] illustrating the wide range of transportation methods which it could influence.
4. Other uses. MCRWPT technology has also been considered to power IoT devices. One implementation has expanded this concept to implement a low-power wide-area network that could provide power to multiple devices [26]. MCRWPT technology has also been adapted for use in metal object detection [27].

In addition to the research aiming to implement MCRWPT technology in existing systems, there is also research being conducted into improving the characteristics of MCRWPT capabilities in general.

One such method of improving the capabilities of MCRWPT technology is to manipulate the operating frequency of the system. One proposed system adjusts the operating frequency via frequency tracking to achieve this [28], while others use a multifrequency system [18, 29]. Unfortunately, any MCRWPT system put into commercial use will have to comply with existing laws regarding the electromagnetic spectrum. As such their operating frequencies will be limited to the ISM bands, making such multifrequency systems unusable [30]

As a result of this limitation, efforts to improve MCRWPT systems are largely focused on improving the magnetic coupling between the coils or altering their impedance. Of these two options, the magnetic coupling approach appears to be the most common. Methods of improving the coupling vary from the use of ferrite on the coils to focus the magnetic field [8, 31] to designing the coils such that they exhibit a higher Q factor [32] or improved electromagnetic properties [10]. On the impedance side, systems have been proposed which use double-end impedance converter networks to improve the coil impedances for different distance transmission [9].

2.3 Discussion

One of the common trends throughout most of the design work being conducted is that the electromagnetic parameters of the coils are the primary focus, while optimal circuit parameters are determined via an optimization routine [8, 19].

In that light, it would be advantageous to have a system which would allow for circuit parameters to be calculated simply, without having to be optimized in ADS, PSpice, or other software. It would also be beneficial if these parameters could be calculated to achieve some form of high efficiency and predictable transmission over a predetermined distance. The merging of filter theory with MCRWPT theory would also allow a resultant system's transmission characteristics to be understood through a transfer function, which would simplify matters.

Chapter 3 MCRWPT and Filter Theory Derivations

In this section, the MCRWPT circuit will be solved to obtain functions for the transfer efficiency and load power. Next, an analog filter which is capable of being implemented by the efficiency function will be derived. Finally, equations that bridge or map the two systems will be identified so that the efficiency of the WPT system may emulate the performance of the filter.

3.1 MCRWPT Derivation

We begin by considering the circuit diagram shown in Figure 3.1.1.

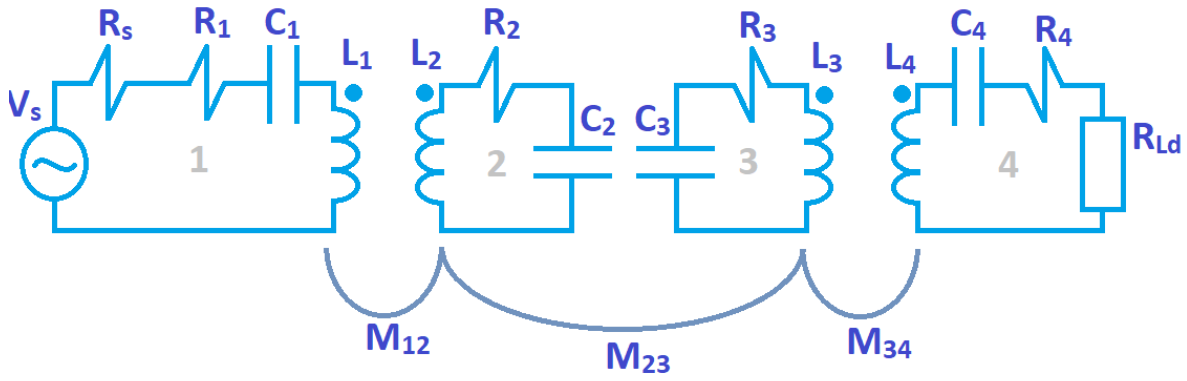

Figure 3.1.1: The Circuit Diagram for the MCRWPT Derivation

The three mutual inductance terms shown are all that will be considered. In a physical system, M_{13}, M_{14}, M_{24} would exist; however, they are considered to be inconsequential compared to M_{12}, M_{23}, and M_{34}, and are thus ignored in the interests of simplifying the circuit.

Capacitors C_1 and C_4 have also been added to the standard circuit described so that the imaginary component of the source/load impedance can be tuned if necessary. If necessary, any capacitor could be replaced by an inductor to satisfy the required conditions.

The resistors, inductors and capacitors in each coil will be combined together into a singular complex impedance parameter for each coil, as described in equation 3.1.1. The source resistance (R_s) and the load resistance (R_{Ld}) are not included in these combined impedance terms. These combined impedance terms were chosen both to limit the number of variables used in the following equations as well as permit a simple removal of the C_1 and C_4 capacitors in the final system if they are deemed to be unnecessary. It will also allow for the conversion of a capacitor to an inductor if the final solution requires it without completely rederiving the equations.

$$R_n + j\omega L_n - \frac{j}{\omega C_n} = Z_n \tag{3.1.1}$$

The MCRWPT system may now be solved, as shown below. Equations 3.1.2 through 3.1.5 show the loop equations for each of the coils.

$$V_s = I_1 R_s + Z_1 I_1 - j\omega M_{12} I_2 \tag{3.1.2}$$

$$0 = Z_2 I_2 - j\omega M_{12} I_1 - j\omega M_{23} I_3 \tag{3.1.3}$$

$$0 = Z_3 I_3 - j\omega M_{23} I_2 - j\omega M_{34} I_4 \tag{3.1.4}$$

$$0 = Z_4 I_4 + I_4 R_{Ld} - j\omega M_{34} I_3 \tag{3.1.5}$$

Next, the voltage observed at the load can be identified.

$$-I_4 R_{Ld} = V_{Ld} = Z_4 I_4 - j\omega M_{34} I_3 \tag{3.1.6}$$

Solving for I_4,

$$I_4 = \frac{-V_{Ld}}{R_{Ld}} \tag{3.1.7}$$

To simplify the following equations by removing unnecessary fractions, R_x is introduced:

$$R_x = \frac{1}{R_{Ld}} \tag{3.1.8}$$

Continuing,

$$I_3 = \frac{(Z_4R_x+1)V_{Ld}}{j\omega M_{34}} \tag{3.1.9}$$

$$I_2 = -\frac{V_{Ld}\left(Z_3(Z_4R_x+1)+\omega^2M_{34}^2R_x\right)}{\omega^2M_{23}M_{34}} \tag{3.1.10}$$

$$I_1 = -\frac{V_{Ld}\left(Z_2\left(Z_3(Z_4R_x+1)+\omega^2M_{34}^2R_x\right)+\omega^2M_{23}^2(Z_4R_x+1)\right)}{j\omega^3M_{12}M_{23}M_{34}} \tag{3.1.11}$$

$$V_s = \frac{-V_{Ld}(Z_1+R_s)\left(Z_2\left(Z_3(Z_4R_x+1)+\omega^2M_{34}^2R_x\right)+\omega^2M_{23}^2Z_3(Z_4R_x+1)+\omega^2M_{12}^2\left(Z_3(Z_4R_x+1)+\omega^2M_{34}^2R_x\right)\right)}{j\omega^3M_{12}M_{23}M_{34}} \tag{3.1.12}$$

In the interests of simplifying the equations for viewing, α and β are introduced.

$$\alpha = Z_2(Z_3(Z_4R_x+1)+\omega^2M_{34}^2R_x)+\omega^2M_{23}^2(Z_4R_x+1)) \tag{3.1.12}$$

$$\beta = \omega^2M_{12}^2(Z_3(Z_4R_x+1)+\omega^2M_{34}^2R_x) \tag{3.1.13}$$

General formulas for load voltage and current, as well as input power and current, can now be identified.

$$V_{Ld} = -\frac{j\omega^3M_{12}M_{23}M_{34}V_s}{(Z_1+R_s)\alpha+\beta} \tag{3.1.14}$$

$$I_{Ld} = -\frac{j\omega^3M_{12}M_{23}M_{34}RxV_s}{(Z_1+R_s)\alpha+\beta} \tag{3.1.15}$$

$$V_{In} = \frac{(Z_1\alpha+\beta)V_s}{(Z_1+R_s)\alpha+\beta} \tag{3.1.16}$$

$$I_{In} = \frac{\alpha V_s}{(Z_1+R_s)\alpha+\beta} \tag{3.1.17}$$

This allows for input and output power to be derived, as well as the power transfer efficiency.

$$P_{Ld} = V_{Ld}I_{Ld}^* = \frac{\omega^6M_{12}^2M_{23}^2M_{34}^2V_s^2R_x}{\left((Z_1+R_s)\alpha+\beta\right)\left((Z_1^*+R_s)\alpha^*+\beta^*\right)} \tag{3.1.18}$$

$$P_{In} = V_{In}I_{In}^* = \frac{(Z_1\alpha+\beta)\alpha^*V_s^2}{\left((Z_1+R_s)\alpha+\beta\right)\left((Z_1^*+R_s)\alpha^*+\beta^*\right)} \tag{3.1.19}$$

$$PTE = \frac{P_{Ld}}{P_{In}} = \frac{\omega^6M_{12}^2M_{23}^2M_{34}^2R_x}{(Z_1\alpha+\beta)\alpha^*} \tag{3.1.20}$$

3.2 Applied Filter Theory

With the power transfer efficiency derived, we can now consider the derivation of the filter transfer function and its application to the MCRWPT system.

In a typical filter system, the output amplitude is dependent on the input frequency. In an MCRWPT system, input frequency is analogous to the distance between coils two and three. However, D_{23} is not a useful filter input due to the complicated relationships between D_{23} and M_{23} which are not constant for all configurations. As such, some form of M_{23} will be the input variable for this filter concept.

One of the primary limitations in applying filter theory to a four coil WPT system is the conversion from a WPT transfer function to a Filter transfer function. The basic form of the PTE function is shown below:

$$PTE = \frac{A_1 M_{23}^2}{A_2 M_{23}^4 + A_3 M_{23}^2 + A_4} \tag{3.2.1}$$

Unlike many conventional filter transfer functions, there are exceptionally few poles and zeros in this equation. As a result, the number and order of potential filters which can be implemented are extremely limited. This also presents the question of what form of M_{23} to use for the input variable. If M_{23} itself is used, the M_{23}^3 and M_{23}^1 terms in the denominator will need to solve to zero as they cannot be replicated in the efficiency function. The use of M_{23} technically allows for higher-order filters to be implemented, but the restrictions on coefficient values may be somewhat limiting.

Alternatively, M_{23}^2 can be used as the input variable. This restricts the potential range of filters that can be implemented, but it also simplifies the process of identifying impedance terms. In this configuration, the only workable system is a pair of cascaded filters – One high pass and one low pass, resulting in a bandpass design.

A Chebyshev design process was used for the high and low pass filters as described in [33]. Based on the PTE function, these must be first-order filters.

$$\epsilon = \sqrt{\frac{1}{|H(j\omega)|^2} - 1} \tag{3.2.2}$$

$$\eta = \sinh\left(\frac{1}{n}\sinh^{-1}\frac{1}{\epsilon}\right) \tag{3.2.3}$$

$$\theta_r = \frac{(2r-1)\pi}{2n} \tag{3.2.4}$$

$$H(s) = \frac{\prod_{r=1}^{n}\left(\eta^2+\sin^2\left(\frac{r\pi}{n}\right)\right)^{\frac{1}{2}}}{\prod_{r=1}^{n}\left(s+\left(\eta\sin\theta_r+j(1+\eta^2)^{\frac{1}{2}}\cos\theta_r\right)\right)} \tag{3.2.5}$$

This leads to the pair of filters described by equations 3.2.6 and 3.2.7. When cascaded together, they form equation 3.2.8. This will be the function which the efficiency function must emulate.

$$HPF(s) = \frac{\eta s}{\omega_h+\eta s} \tag{3.2.6}$$

$$LPF(s) = \frac{\eta\omega_l}{s+\eta\omega_l} \tag{3.2.7}$$

$$BPF(s) = \frac{\eta^2\omega_l s}{\eta s^2+(\omega_h+\eta^2\omega_l)s+\eta\omega_l\omega_h} \tag{3.2.8}$$

3.3 The Bridging or Mapping Equations

The connections between the efficiency function and the bandpass filter are realized using the bridging or mapping equations. Eventually, these equations will be solved algebraically for individual resistances or reactances, allowing for the filter design to be implemented in hardware.

The four impedance variables, their corresponding resistances and reactances and the mutual coupling between coils two and three are considered to be the user-selected or calculated variables. All other variables, such as M_{12}, M_{34}, load or source resistances and the operating frequency are parameters that will be defined by the user and will not be altered further by this design process. This decision was made to ensure that solutions generated through this process would be compatible with a wide range of existing coils and standards.

None of the solutions present in this thesis have been optimized. Individual configurations could be optimized by users; however, given that any optimization will depend on the coil-specific parameters of M_{12} and M_{34} as well as the operating frequency, solution optimization is considered to be beyond the scope of this thesis.

Unlike the variables in the denominator of equation 3.2.1, the variable in the numerator is only dependant on mutual coupling, operating frequency, and load resistance. These terms could be manipulated to achieve the desired relationship; however, this may not be possible in an existing system. As such, equation 3.1.2 is multiplied by a scaling variable, resulting in equation 3.3.1

$$PTE = \frac{\omega^6 M_{12}^2 M_{23}^2 M_{34}^2 R_x B}{(Z_1\alpha+\beta)\alpha^* B} \tag{3.3.1}$$

Solving the denominator and breaking the equations into the coefficients from equation 3.2.1 leads to equations 3.3.2 through 3.3.5.

$$A_1 = \omega^6 M_{12}^2 M_{34}^2 R_x B \tag{3.3.2}$$

$$A_2 = Z_1 \omega^4 (Z_4 R_x + 1)(Z_4^* R_x + 1) B \tag{3.3.3}$$

$$A_3 = ((Z_1 Z_2 + \omega^2 M_{12}^2)(Z_3(Z_4 R_x + 1) + \omega^2 M_{34}^2 R_x)\omega^2 (Z_4^* R_x + 1) + \omega^2 (Z_4 R_x + 1)\big(Z_2^*(Z_3^*(Z_4^* R_x + 1) + \omega^2 M_{34}^2 R_x)\big))B \tag{3.3.4}$$

$$A_4 = \big(Z_1 Z_2 (Z_3(Z_4 R_x + 1) + \omega^2 M_{34}^2 R_x) + \omega^2 M_{12}^2 (Z_3(Z_4 R_x + 1) + \omega^2 M_{34}^2 R_x)\big) Z_2^*(Z_3^*(Z_4^* R_x + 1) + \omega^2 M_{34}^2 R_x)\, B \tag{3.3.5}$$

Based on the filter transfer function from section 3.2, the following equivalences are known:

$$A_1 = j\eta^2 \omega_l \tag{3.3.6}$$

$$A_2 = -\eta \tag{3.3.7}$$

$$A_3 = j(\eta^2 \omega_l + \omega_h) \tag{3.3.8}$$

$$A_4 = \eta \omega_l \omega_h \tag{3.3.9}$$

Combining equations 3.3.6 and 3.3.2 allows for B to be identified.

$$B = \frac{j\eta^2 \omega_l}{\omega^6 M_{12}^2 M_{34}^2 R_x} \tag{3.3.10}$$

In the interest of simplifying the eventual solution, it is convenient to break the four impedance terms into resistances and reactances.

$$Z_n = R_n + jX_n \tag{3.3.11}$$

Solving the A_2 equation in 3.3.12 leads to equations 3.3.13 and 3.3.14 for the real and imaginary bridging equations.

$$-\eta = \frac{Z_1 \omega^4 (Z_4 R_x + 1)(Z_4^* R_x + 1) j\eta^2 \omega_l}{\omega^6 M_{12}^2 M_{34}^2 R_x} \tag{3.3.12}$$

$$\eta = \frac{\omega^4 \eta^2 \omega_l X_1 (R_4^2 R_x^2 + X_4^2 R_x^2 + 2R_4 R_x + 1)}{\omega^6 M_{12}^2 M_{34}^2 R_x} \tag{3.3.13}$$

$$0 = \frac{\omega^4\eta^2\omega_l R_1(R_4^2R_x^2+X_4^2R_x^2+2R_4R_x+1)}{\omega^6M_{12}^2M_{34}^2R_x} \quad (3.3.14)$$

Next, the A_3 equation may be solved, which leads to equations 3.3.15 and 3.3.16.

$$0 = \frac{2X_1\eta^2\omega_l}{\omega^4M_{12}^2M_{34}^2R_x}(R_4^2R_x^2 + X_4^2R_x^2 + 2R_4R_x + 1)(X_2X_3 - R_2R_3) - \frac{X_3\eta^2\omega_l}{\omega^2M_{34}^2R_x}(R_4^2R_x^2 + X_4^2R_x^2 + 2R_4R_x + 1) - \frac{2X_1\eta^2\omega_l}{\omega^2M_{12}^2}(R_2 + R_2R_4R_x + X_2X_4R_x) + X_4R_x\eta^2\omega_l \quad (3.3.15)$$

$$\eta^2\omega_l + \omega_h = \frac{2R_1\eta^2\omega_l}{\omega^4M_{12}^2M_{34}^2R_x}(R_4^2R_x^2 + X_4^2R_x^2 + 2R_4R_x + 1)(R_2R_3 - X_2X_3) + \frac{R_3\eta^2\omega_l}{\omega^2M_{34}^2R_x}(R_4^2R_x^2 + X_4^2R_x^2 + 2R_4R_x + 1) + \frac{2R_1\eta^2\omega_l}{\omega^2M_{12}^2}(R_2 + R_2R_4R_x + X_2X_4R_x) + \eta^2\omega_l(R_4R_x + 1) \quad (3.3.16)$$

Finally, the A_4 equation may be solved.

$$\eta^2\omega_l\omega_h = \frac{\eta^2\omega_l\left(X_2\omega^2M_{12}^2 - X_1\left(R_2^2+X_2^2\right)\right)}{\omega^4M_{12}^2}\left(\frac{\left(X_3^2+R_3^2\right)\left(R_4^2R_x^2+X_4^2R_x^2+2R_4R_x+1\right)}{\omega^2M_{34}^2R_x} + 2R_3R_4 - 2X_3X_4 + 2R_3 + \omega^2M_{34}^2R_x\right) \quad (3.3.17)$$

$$0 = \frac{\eta^2\omega_l\left(R_2\omega^2M_{12}^2 + R_1\left(R_2^2+X_2^2\right)\right)}{\omega^4M_{12}^2}\left(\frac{\left(X_3^2+R_3^2\right)\left(R_4^2R_x^2+X_4^2R_x^2+2R_4R_x+1\right)}{\omega^2M_{34}^2R_x} + 2R_3R_4 - 2X_3X_4 + 2R_3 + \omega^2M_{34}^2R_x\right) \quad (3.3.18)$$

The bridging equations may now be solved for individual resistances or reactances. This will be completed in Section 4.

Chapter 4 Solutions to the Bridging or Mapping Equations

At this stage, eight variables and six different equations have been identified. This presents the possibility of approximately twenty thousand different solutions to the bridging equations. Fortunately, the constraints put in place by the equations greatly reduce this number.

In the final solution, a user should be able to define their system's parameters (such as mutual coupling) as well as two of these variables. The solutions to the bridging equations should then determine the remaining six variables. Direct solutions are preferable whenever possible to simplify these calculations.

Each of the variables must be wholly real in order to satisfy the conditions of the bridging equations. In addition, all resistance terms must be greater than zero to be physically realizable.

Table 4.1 shows the variables present in each of the bridging equations. The cells which are highlighted correspond to values from the transfer function. The non-highlighted cells should be zero.

Table 4.1: The Variables Present in each Bridging Equation

	M_{23}^4	M_{23}^2	M_{23}^0
Real Part	X_1, R_4, X_4	$R_1, X_1, R_2, X_2, R_3, X_3, R_4, X_4$	$R_1, X_1, R_2, X_2, R_3, X_3, R_4, X_4$
Imaginary Part	R_1, R_4, X_4	$R_1, X_1, R_2, X_2, R_3, X_3, R_4, X_4$	$R_1, X_1, R_2, X_2, R_3, X_3, R_4, X_4$

4.1 Solution Limitations

Before any of the bridging functions are solved, the limitations to any solution must be addressed. These limitations are most visible when the real and imaginary parts of the M_{23}^4 equation are examined together.

$$\eta + 0j = \frac{\omega^4 \eta^2 \omega_l (jR_1 + X_1)(R_4^2 R_x^2 + X_4^2 R_x^2 + 2R_4 R_x + 1)}{\omega^6 M_{12}^2 M_{34}^2 R_x} \quad (4.1.1)$$

Equation 4.1.1 is clearly unrealizable unless R_1 is zero. This is impossible, however, as R_1 is the resistance of the driver coil. This means that the efficiency function cannot be made to match the filter transfer function perfectly.

Alternatively, the efficiency function can be made to approximate the filter transfer function. To do this, the undesirable terms in the function must be made small enough that they will not greatly affect the performance of the final system.

Figure 4.1.1 shows the amplitude of an ideal filter transfer function as a function of M_{23}^2. In this configuration, $\omega_h = 3.7854 * 10^{-22}$, $\omega_l = 1.6205 * 10^{-16}$, and $\eta = 3.0424$. Figure 4.1.2 shows an approximated version of this transfer function where every term in the denominator has an undesired term attached with a magnitude of $\pm 10\%$ of the desired term. Figure 4.1.3 shows a closer view of the passband magnitude.

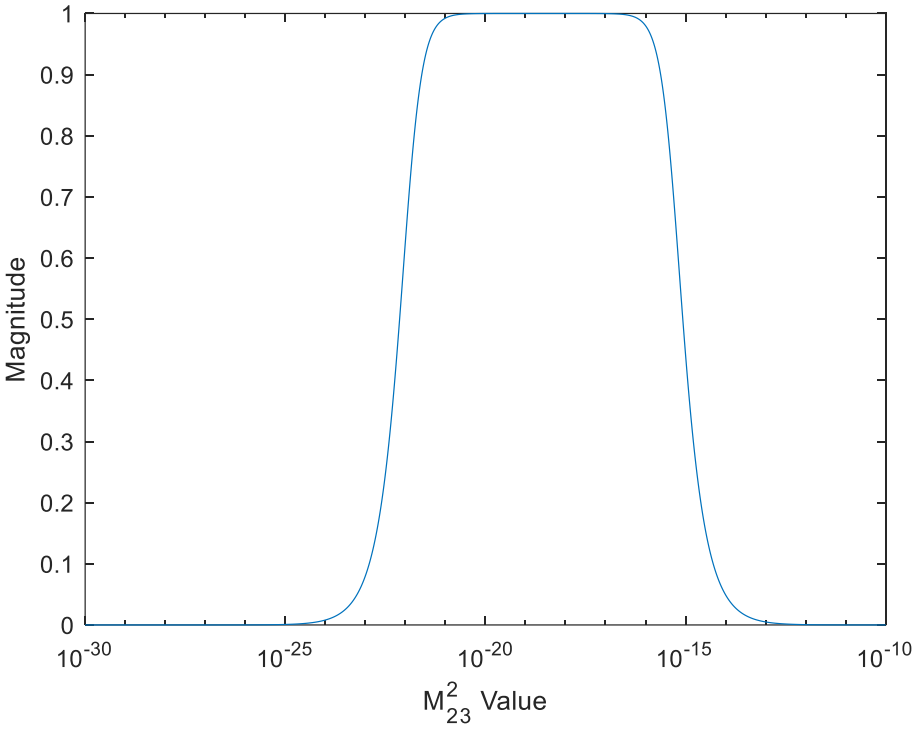

Figure 4.1.1: The Ideal Transfer Function

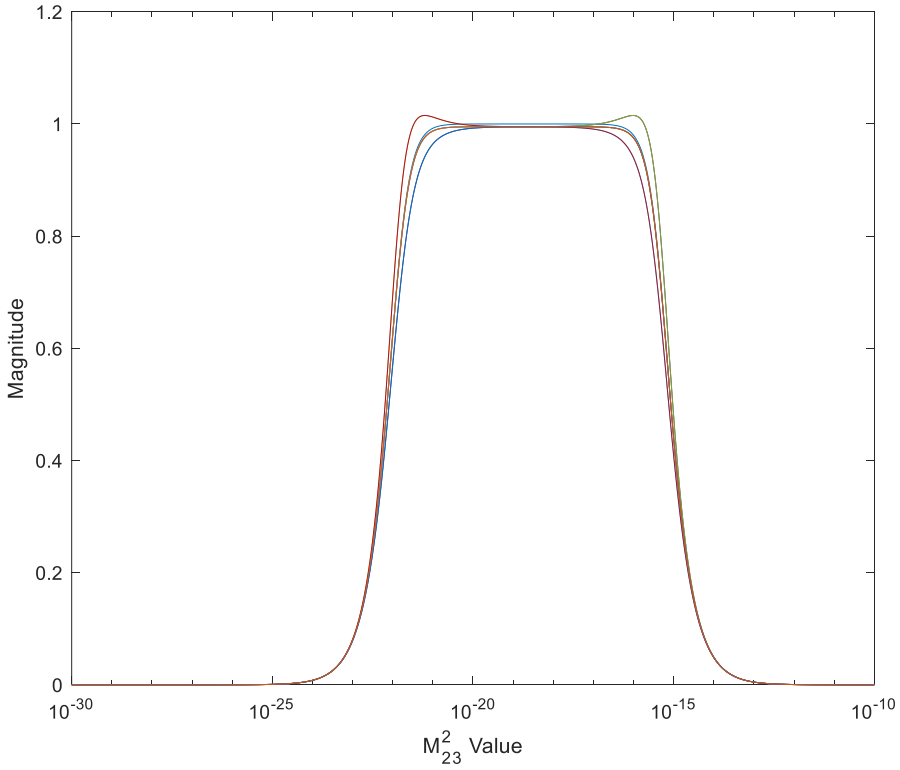

Figure 4.1.2: The Approximated Transfer Functions

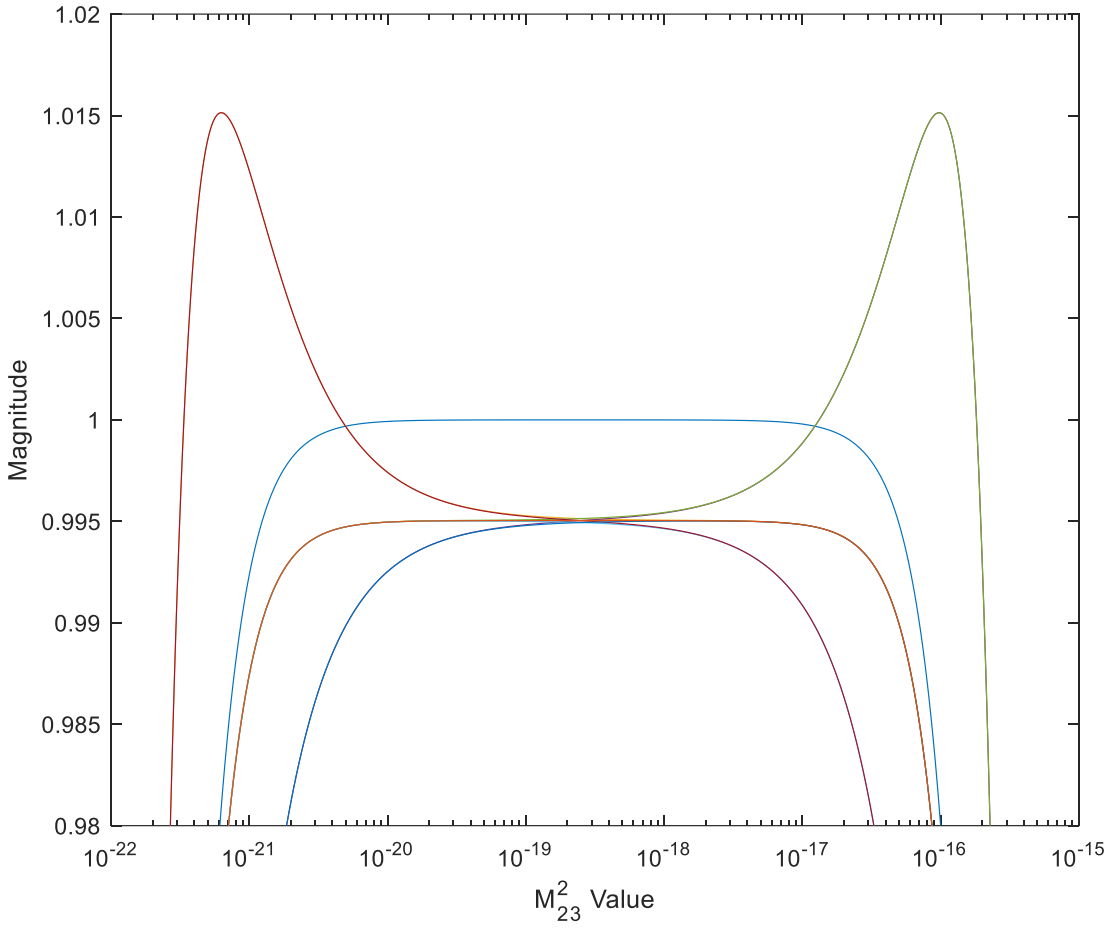

Figure 4.1.3: Enhanced View of the Approximated Transfer Function Passband

Of the eight different approximated transfer functions shown in Figure 4.1.3, the two traces which peak at a magnitude of approximately 1.015 are likely unachievable due to the lack of amplification and the requirement that all circuit component be physically implementable. The remaining six exhibit a smaller passband than the ideal transfer function, and a lower maximum achievable efficiency. However, while the approximated filters are not perfect, a loss of 0.5% efficiency is completely acceptable. As such, all tests were conducted assuming that the undesired terms were no more than 10% of the magnitude of the desired terms in the transfer function.

4.2 General Solution to the Bridging Functions

The first solution to be considered will be a general solution. As it was previously stated, there are approximately twenty thousand solutions to an eight permutation six problem. The actual number of solutions will be lower as all eight variables are not present in each equation; however, there is still a multitude of potential solutions in existence. As such, the solution which will eventually be derived is not considered to be the only correct solution to the bridging equations. It is also not necessarily the best possible solution to these equations. This is a solution that is physically achievable.

The M_{23}^4 equations will be solved first. Recalling equation 4.1.1 and inserting the undesired term yields equation 4.2.1.

$$\eta\left(1+\frac{j}{10\gamma_2}\right)=\frac{\omega^4\eta^2\omega_\iota(jR_1+X_1)(R_4^2R_x^2+X_4^2R_x^2+2R_4R_x+1)}{\omega^6M_{12}^2M_{34}^2R_x} \tag{4.2.1}$$

γ_2 has been added as a scaling factor in equation 4.1.1. This allows for the undesired term to be made smaller if the need arises without completely rederiving the equations. The two subscripts indicate that this controls the relationship between the parts of the S^2 term. The limitations placed on γ_2 are shown in equation 4.2.2.

$$|\gamma_2|\geq 1 \tag{4.2.2}$$

As was noted previously, the second bracketed term in equation 4.2.1 is a scalar which exists in both the real and imaginary parts of equation 4.2.1. This means that the relationship between R_1 and X_1 will control the relationship between the desired and undesired terms. This leads to the relationship shown in equation 4.2.3.

$$X_1 = 10\gamma_2 R_1 \tag{4.2.3}$$

Next, the real part of equation 4.2.1 is considered. This creates a relationship between X_1, R_4, and X_4. Given that a simple relationship exists between X_1 and R_1, and these terms appear in every other bridging equation, X_1 is chosen to be one of the user-chosen variables. R_4 will be the second. This allows for X_4 to be identified in equation 4.2.4.

$$X_4 = \pm \frac{\sqrt{\frac{\omega^2 M_{12}^2 M_{34}^2 R_x}{\eta \omega_l X_1} - R_4^2 R_x^2 - 2R_4 R_x - 1}}{R_x} \tag{4.2.4}$$

Before the next bridging equation is solved, a useful substitution should be presented. The $(Z_4 R_x + 1)(Z_4^* R_x + 1)$ term appears in each of the bridging functions. This means that the scalar term in equation 4.2.1 appears multiple times throughout the derivation. In the interests of simplifying the math conducted by a user, equation 4.2.5 allows for this term to be substituted for a simpler term.

$$\frac{\omega^2 M_{12}^2 M_{34}^2 R_x}{\eta \omega_l X_1} = (R_4^2 R_x^2 + X_4^2 R_x^2 + 2R_4 R_x + 1) \tag{4.2.5}$$

The M_{23}^2 bridging equation will be solved for R_3 and X_3. The real part will be solved for X_3, while the imaginary part will be solved for R_3. First, the substitutions presented in equations 4.2.3 and 4.2.5 will be applied to equations 3.3.15 and 3.3.16, leading to equations 4.2.6 and 4.2.7, respectively.

$$0 = \frac{2\eta}{\omega^2}(X_2 X_3 - R_2 R_3) - \frac{X_3 \eta M_{12}^2}{X_1} - \frac{2X_1 \eta^2 \omega_l}{\omega^2 M_{12}^2}(R_2 + R_2 R_4 R_x + X_2 X_4 R_x) + X_4 R_x \eta^2 \omega_l \tag{4.2.6}$$

$$\eta^2 \omega_l + \omega_h = \frac{\eta^2}{5\gamma_2 \omega^2}(R_2 R_3 - X_2 X_3) + \frac{R_3 \eta M_{12}^2}{X_1} + \frac{2R_1 \eta^2 \omega_l}{\omega^2 M_{12}^2}(R_2 + R_2 R_4 R_x + X_2 X_4 R_x) + \eta^2 \omega_l (R_4 R_x + 1) \tag{4.2.7}$$

Setting equation 4.2.6 equal to $\frac{\eta^2\omega_l+\omega_h}{10\gamma_1}$ and solving for X_3 results in equation 4.2.8. Similarly, equation 4.2.7 can be solved for R_3 which creates equation 4.2.9.

$$X_3 = \frac{\frac{\eta^2\omega_l+\omega_h}{10\gamma_1}+\frac{2X_1\eta^2\omega_l}{\omega^2M_{12}^2}(R_2+R_2R_4R_x+X_2X_4R_x)+\frac{2\eta R_2R_3}{\omega^2}-X_4R_x\eta^2\omega_l}{\frac{2\eta X_2}{\omega^2}-\frac{\eta M_{12}^2}{X_1}} \tag{4.2.8}$$

$$R_3 = \frac{\eta^2\omega_l+\omega_h-\frac{2R_1\eta^2\omega_l}{\omega^2M_{12}^2}(R_2+R_2R_4R_x+X_2X_4R_x)-\eta^2\omega_l(R_4R_x+1)+\frac{\eta^2X_2X_3}{5\gamma_2\omega^2}}{\frac{R_2\eta^2}{5\gamma_2\omega^2}+\frac{\eta M_{12}^2}{X_1}} \tag{4.2.9}$$

Finally, the M_{23}^0 equations may be solved for R_2 and X_2. Once again, the substitutions presented in equations 4.2.3 and 4.2.5 will be applied. This leads to equation 3.3.17 becoming equation 4.2.10, and equation 3.3.18 becomes equation 4.2.11.

$$\eta^2\omega_l\omega_h = \frac{\eta^2\omega_l\left(X_2\omega^2M_{12}^2-X_1\left(R_2^2+X_2^2\right)\right)}{\omega^4M_{12}^2}\left(\frac{\left(X_3^2+R_3^2\right)M_{12}^2}{\eta\omega_lX_1}+2R_3R_4-2X_3X_4+2R_3+\omega^2M_{34}^2R_x\right) \tag{4.2.10}$$

$$0 = \frac{\eta^2\omega_l\left(R_2\omega^2M_{12}^2+\frac{X_1\left(R_2^2+X_2^2\right)}{10\gamma_2}\right)}{\omega^4M_{12}^2}\left(\frac{\left(X_3^2+R_3^2\right)M_{12}^2}{\eta\omega_lX_1}+2R_3R_4-2X_3X_4+2R_3+\omega^2M_{34}^2R_x\right) \tag{4.2.11}$$

Equation 4.2.10 is solved for X_2 while equation 4.2.11 is set equal to $\frac{\eta^2\omega_l\omega_h}{10\gamma_0}$ and solved for R_2. This leads to equations 4.2.12 and 4.2.13, respectively.

$$X_2 = \frac{-\omega^2M_{12}^2 \pm \sqrt{\omega^4M_{12}^4+\frac{4X_1\omega_h\omega^4M_{12}^2}{\left(\frac{\left(X_3^2+R_3^2\right)M_{12}^2}{\eta\omega_lX_1}+2R_3R_4-2X_3X_4+2R_3+\omega^2M_{34}^2R_x\right)}+4X_1^2R_2^2}}{-2X_1} \tag{4.2.12}$$

$$R_2 = \frac{-\omega^2M_{12}^2 \pm \sqrt{\omega^4M_{12}^4-\frac{X_1\omega_h\omega^4M_{12}^2}{25\gamma_2\gamma_0\left(\frac{\left(X_3^2+R_3^2\right)M_{12}^2}{\eta\omega_lX_1}+2R_3R_4-2X_3X_4+2R_3+\omega^2M_{34}^2R_x\right)}-\frac{X_1^2X_2^2}{25\gamma_2^2}}}{\frac{X_1}{5\gamma_2}} \tag{4.2.13}$$

Experimental trials using these equations has shown that both equations 4.2.12 and 4.2.13 yield preferable results when the roots are added. As such, equations 4.2.12 and 4.2.13 are restated in equation 4.2.14 and 4.2.15.

$$X_2 = \frac{-\omega^2 M_{12}^2 + \sqrt{\omega^4 M_{12}^4 + \frac{4X_1\omega_h\omega^4 M_{12}^2}{\left(\frac{(X_3^2+R_3^2)M_{12}^2}{\eta\omega_l X_1} + 2R_3R_4 - 2X_3X_4 + 2R_3 + \omega^2 M_{34}^2 R_x\right)} + 4X_1^2R_2^2}}{-2X_1} \tag{4.2.14}$$

$$R_2 = \frac{-\omega^2 M_{12}^2 + \sqrt{\omega^4 M_{12}^4 - \frac{X_1\omega_h\omega^4 M_{12}^2}{25\gamma_2\gamma_0\left(\frac{(X_3^2+R_3^2)M_{12}^2}{\eta\omega_l X_1} + 2R_3R_4 - 2X_3X_4 + 2R_3 + \omega^2 M_{34}^2 R_x\right)} - \frac{X_1^2X_2^2}{25\gamma_2^2}}}{\frac{X_1}{5\gamma_2}} \tag{4.2.15}$$

This marks the completion of the general solution to the bridging equations. The implementation of this solution will be described in section 4.3.

4.3 Implementation of the General Solution

Now that the general solution has been identified, it can be used to produce circuit component values for a given system.

A user may either be with a set of known coils which will be modified to fit the required parameters or by specifying certain characteristics which will be implemented physically after the design process. The second option may require an iterative approach to the design process until all characteristics mesh together.

The user is required to provide values for M_{12}, M_{34}, ω_l, ω_h and the maximum passband attenuation, which will determine η. These values will vary depending on the coil design and desired separations.

Once these values have been determined, X_1 and R_4 maybe selected. These variables are constrained by the calculation for X_4 in equation 4.2.4 as they appear within a square root and thus must be chosen such that X_4 is wholly real. This limitation is described in equation 4.3.1.

$$\frac{\omega^2 M_{12}^2 M_{34}^2 R_x}{\eta \omega_l X_1} - R_4^2 R_x^2 - 2R_4 R_x \geq 1 \tag{4.3.1}$$

Solving equation 4.3.1 for R_4 will provide an acceptable range of values for R_4 at any given value of X_1. The solution is shown in equation 4.3.2.

$$R_{4Lim} = \frac{1 \pm \omega M_{12} M_{34} \sqrt{\frac{R_x}{\eta \omega_l X_1}}}{-R_x} \tag{4.3.2}$$

Given that R_4 represents the resistance of the load coil, it cannot be less or equal to zero. As such, equation 4.3.2 may be restated into equation 4.3.3.

$$R_{4_{Max}} = \frac{\left(1 - \omega M_{12} M_{34} \sqrt{\frac{R_x}{\eta \omega_l X_1}}\right)}{-R_x} \tag{4.3.3}$$

Equation 4.3.3 also indicates that there is a limit to how large X_1 can be. This is illustrated in equation 4.3.4.

$$X_{1_{Max}} = \frac{\omega^2 M_{12}^2 M_{34}^2 R_x}{\eta \omega_l} \tag{4.3.4}$$

Figure 4.3.1 shows a sample of the restrictions existing on X_1 and R_4. In this sample, $M_{12} = M_{34} = 1.1675 * 10^{-7}$, $\omega_l = 1.6205 * 10^{-16}$, and the maximum passband attenuation is set to 5%, meaning that $\eta = 3.0424$.

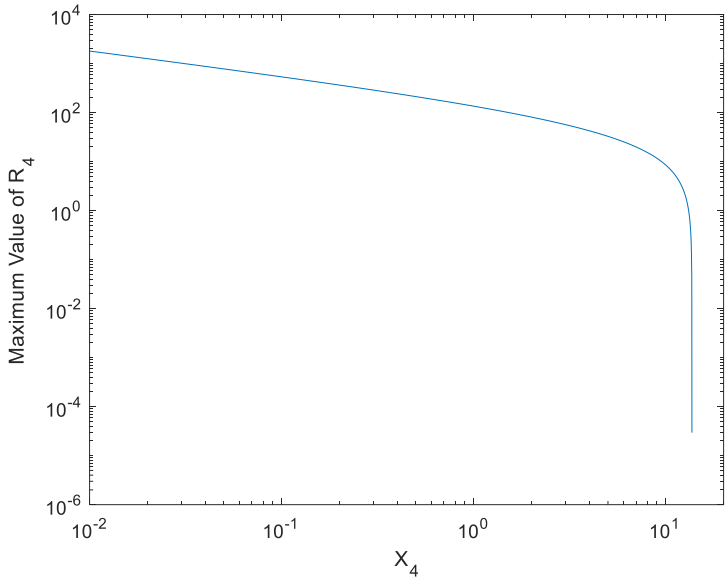

Figure 4.3.1: Maximum Value of R_4 as a function of X_4

According to Figure 4.3.1, the absolute maximum acceptable value for X_1 in this scenario is 13.68. This matches the maximum value calculated using equation 4.3.4.

Once X_1 and R_4 have been selected, X_4 may be calculated using equation 4.2.4.

Next, the values for the impedance of the two resonance coils will be calculated. Unlike the previous variables, the final values for these impedances will be obtained through iteration. The user begins by guessing values for R_2, X_2, and R_3. Generally, these values may be set equal to R_1. If unsuccessful, set each value to 10^{-10}. Once the values are set, the user will calculate X_3, R_3, R_2 and then X_2. If each of the calculated values is physically realizable, and none of the values has changed by more than 10%, the process is considered to be complete. If any of these conditions are not met, the four variables should be recalculated in the same order until their values are satisfactory.

It is important to note that the first few iterations may result in negatives resistances which are physically impossible. If this occurs, another iteration should be conducted. Negative resistance calculations are not uncommon and are usually the result of the initial guess. They are usually eliminated in the next iteration. Processes that produce negative resistances in one iteration usually go on to produce positive resistances in subsequent iterations and ultimately yield successful designs in most cases.

Figure 4.3.2 shows a general flow chart for this design process.

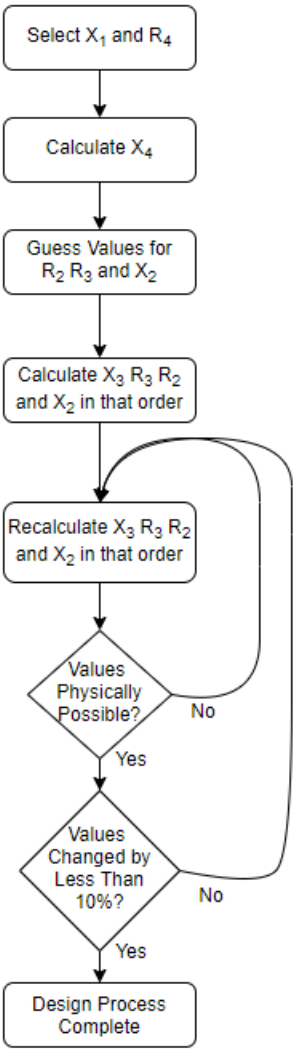

Figure 4.3.2: Flow Chart for the Design Process of the General Solution

4.4 Considerations made in the Design of the General Solution

The variables which were derived in the real and imaginary parts of each bridging equation are shown in Table 4.4.1. The desirable components for each bridging equation are highlighted.

Table 4.4.1: The Variables Derived from Each Section of the Bridging Equations

	M_{23}^4	M_{23}^2	M_{23}^0
Real Part	X_4	X_3	X_2
Imaginary Part	R_1	R_3	C_2

The range variables which may be obtained from the M_{23}^{4} the bridging (or mapping) equation is extremely limited as none of the impedance terms related to the resonance coils appear in this equation. Furthermore, any solution for R_4 and X_4 will depend on either of R_1 or X_1 in addition to the unchosen load coil impedance component. This naturally leads to one each of the driver coil and the load coil impedance components being chosen as user-specified variables. This choice is largely arbitrary as the relationship between the impedance components of the driver coil is extremely simple, and any solution for a load coil parameter will result in a square root which presents the potential for an undesired complex impedance parameter solution.

Users may wish to specify R_1 instead of X_1 to simplify their coil design as it is easier to alter the reactance of a coil than its resistance. X_1 has been chosen in this document as it would allow for the reactance to easily be made negative if desired, which R_1 is incapable of. However, given the existence of the γ_2 term and the previously mentioned simplicity of the relationship between the driver coil impedance terms, this reasoning is largely moot.

The decision for the placement of the resonant coil impedance terms was based on an exhaustive examination of the 96 different potential placements. A complete list of formulas was derived symbolically in Matlab. Individual formulas were then selected from that list, combined, and tested with a small variety of X_1 and R_4 inputs. Unfortunately, most of these combinations were deemed unsuitable for use as the result of several iterations was either divergent or produced complex or impossible physical characteristics.

Combinations that did not contain either of these flaws were then examined in more detail and with multiple different coils and filter configurations. The general solution presented here was found to be acceptable over the widest range of coil and filter combinations.

4.5 Alternative Solution

In the process of deriving the general solution, an additional modified solution was found. The root of this solution is derived from the general solution, however several terms from the R_2 and X_2 equations were falsely eliminated when the sign of one of these terms was flipped. After the algebraic error was identified, the solution was tested and found to have several differences from the general solution. The primary advantage of this solution is that it allows for the region of peak power to be adjusted without negatively affecting the amount of power being transmitted. This will be shown further in Section 5.2.

This alternative solution uses the same inputs as the general solution but does not perfectly reproduce the intended filter transfer function as the high pass characteristics vary depending on the impedance values chosen.

This solution maintains the existing methodology for R_1, X_1, R_4, and X_4. The revised formulas for R_2, X_2, R_3, and X_3 are shown below.

$$R_2 = \frac{-\omega^2 M_{12}^2 + \sqrt{\omega^4 M_{12}^4 + \frac{X_1 \omega_h \omega^4}{25\gamma_2\gamma_0\eta\left(\frac{R_3^2+X_3^2}{\eta\omega_l X_1} + \omega^2 M_{34}^2 R_x\right)} - \frac{X_1^2 X_2^2}{25\gamma_2^2}}}{\frac{X_1}{5\gamma_2}} \tag{4.5.1}$$

$$X_2 = \frac{-\omega^2 M_{12}^2 + \sqrt{\omega^4 M_{12}^4 - \frac{4X_1 \omega_h \omega^4}{\eta\left(\frac{R_3^2+X_3^2}{\eta\omega_l X_1} + \omega^2 M_{34}^2 R_x\right)} - 4X_1^2 R_2^2}}{2X_1} \tag{4.5.2}$$

$$R_3 = \frac{R_{3N}}{R_{3D}} \tag{4.5.3}$$

$$R_{3N} = \omega_h - R_4 R_x \eta^2 \omega_l - \frac{2\eta^2 \omega_l}{\omega^2 M_{12}^2}(X_1 X_2 + R_1 R_2 R_4 R_x + R_1 X_2 X_4 R_x) + \frac{\eta X_2 X_3}{5\gamma_2 \omega^2} -$$

$$\frac{2\eta^2 \omega_l}{\omega^4 M_{12}^2 M_{34}^2 R_x}(R_1 X_2 X_3 (R_4 R_x + 1) + X_1 R_2 X_3 + R_1 R_2 X_3 X_4 R_x + X_1 R_2 X_3 R_4 R_x) \tag{4.5.4}$$

$$R_{3D} = \frac{\eta M_{12}^2}{X_1} + \frac{2\eta}{\omega^2 X_1} - \frac{2\eta^2 \omega_l (R_4 R_x + 1)}{\omega^4 M_{12}^2 M_{34}^2 R_x} + \frac{2\eta^2 \omega_l \left(X_1 X_2 (R_4 R_x + 1) + X_4 R_x (X_1 R_2 + R_1 X_2)\right)}{\omega^4 M_{12}^2 M_{34}^2 R_x} \tag{4.5.5}$$

$$X_3 = \frac{X_{3N}}{X_{3D}} \tag{4.5.6}$$

$$X_{3N} = X_4 R_x \eta^2 \omega_l - \frac{\eta^2 \omega_l + \omega_h}{10\gamma_1} - \frac{2R_2 R_3 \eta}{\omega^2} - \frac{2\eta^2 \omega_l (X_1 R_2 R_4 R_x + X_1 X_2 X_4 R_x - R_1 X_2)}{\omega^2 M_{12}^2} +$$

$$\frac{2\eta^2 \omega_l R_3 (X_1 R_2 (R_4 R_x + 1) - X_4 R_x (X_1 X_2 - R_1 R_2) - R_1 X_2 R_4 R_x)}{\omega^4 M_{12}^2 M_{34}^2 R_x} \tag{4.5.7}$$

$$X_{3D} = \frac{\eta M_{12}^2}{X_1} - \frac{2X_2 \eta}{\omega^2} + \frac{2\eta^2 \omega_l \left((X_1 X_2 - R_1 R_2)(R_4 R_x + 1) + X_4 R_x (X_1 R_2 + R_1 X_2)\right)}{\omega^4 M_{12}^2 M_{34}^2 R_x} \tag{4.5.8}$$

The formulas for R_2 and X_2 are nearly identical. Other than a few sign changes, the largest difference appears in the denominator of the second term within the root where three terms have been removed. The formulas for R_3 and X_3, on the other hand, are completely different. However, as it will be shown in section 5, they are effective at exceeding the filter requirements.

Chapter 5 Simulations of Solutions to the Bridging Equations

The general solutions and design methodology described in section 4 will now be implemented. Simulations were conducted using Matlab as well as Agilent's Advanced Design System. Physical tests were not conducted due to ongoing Covid-19 restrictions.

5.1 Simulations of the General Solution

The first simulation, which will be conducted, uses a pair of the coils shown in Figure 5.1. The physical parameters of these coils are described in Table 5.1.1. Their electrical parameters and the filter parameters used are listed in Table 5.1.2.

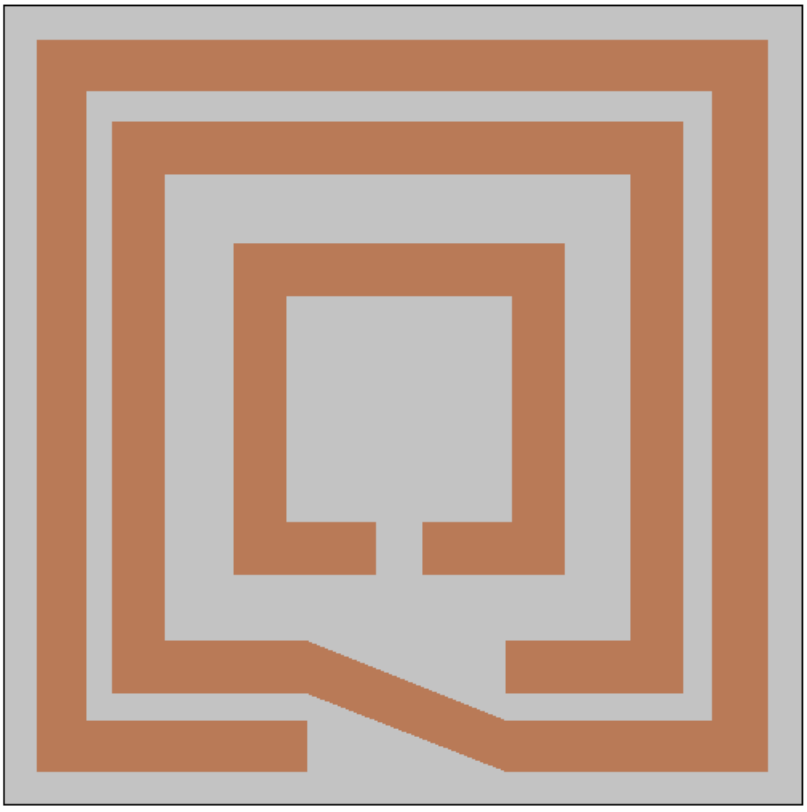

Figure 5.1.1: The Coil

Table 5.1.1: The Physical Parameters of the Coils

Parameter	Inner Coil Value	Outer Coil Value
Outer Radius	3 cm	5 cm
Inner Radius	2.6 cm	3.4 cm
Trace Width	4 mm	6 mm
Gap Width	N/A	4 mm
Trace Thickness	3.47×10^{-2} mm	3.47×10^{-2} mm
Number of Turns in Coil	1	2
Gap in Coil for Connections	3 mm	1 cm

Table 5.1.2: The Electrical and Filter Parameters of the Coils

Parameter	Value
L_1, L_4	75.522 nH
L_2, L_3	325.06 nH
M_{12}	1.1675×10^{-7}
M_{34}	1.1675×10^{-7}
ω_l	$7.2213 * 10^{-20}$ (30 cm)
ω_h	$3.785 * 10^{-22}$ (1 m)
Maximum Passband Attenuation	0.95
X_1	5
R_4	0.01

Inputting the parameters specified by Tables 5.1.1 and 5.1.2 into the general solution results in the six impedance components described by Table 5.1.3. This allows for the values of the added reactive components to be calculated. These values are shown in table 5.1.4.

Table 5.1.3: The Calculated Impedance Components

Parameter	Value
R_1	0.5
R_2	8.4162×10^{-4}
R_3	2.4006×10^{-8}
X_2	8.445×10^{-3}
X_3	6.306×10^{-3}
X_4	3.9175×10^{3}

Table 5.1.4: The Added Reactive Components

Parameter	Value
Inductor (Coil One)	41.849 nH
Capacitor (Coil Two)	1.6862 nF
Capacitor (Coil Three)	1.6960 nF
Inductor (Coil Four)	91.884 μH

The impedances components chosen and calculated in Tables 5.1.3 and 5.1.4 were used in a Matlab script to assess the performance of this system. Figure 5.1.2 shows the magnitude of the power transfer efficiency and the amount of power transmitted as a function of distance. Figure 5.1.3 shows these same plots as a function of M_{23}. Once the system was simulated in Matlab, the same simulation was repeated in ADS. These results are shown in Figures 5.1.4 and 5.1.5.

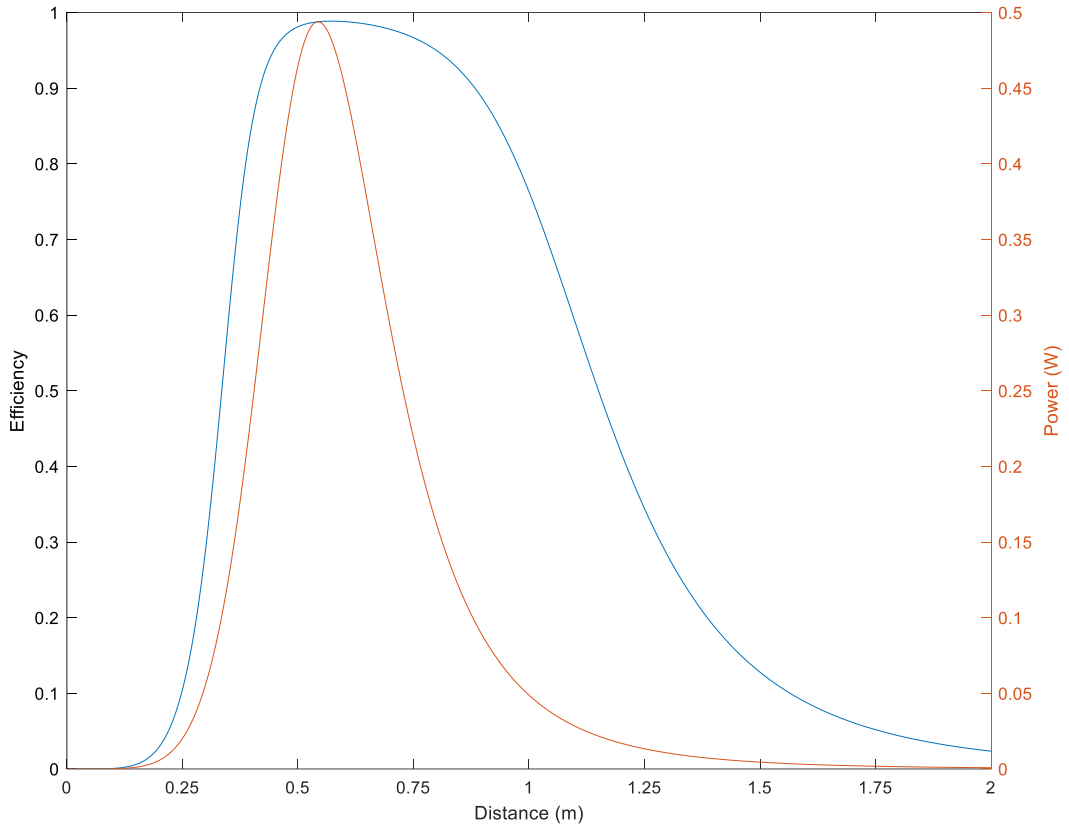

Figure 5.1.2: The Power Transfer Efficiency and Transmitted Power as a Function of Distance ($X_1 = 5$)

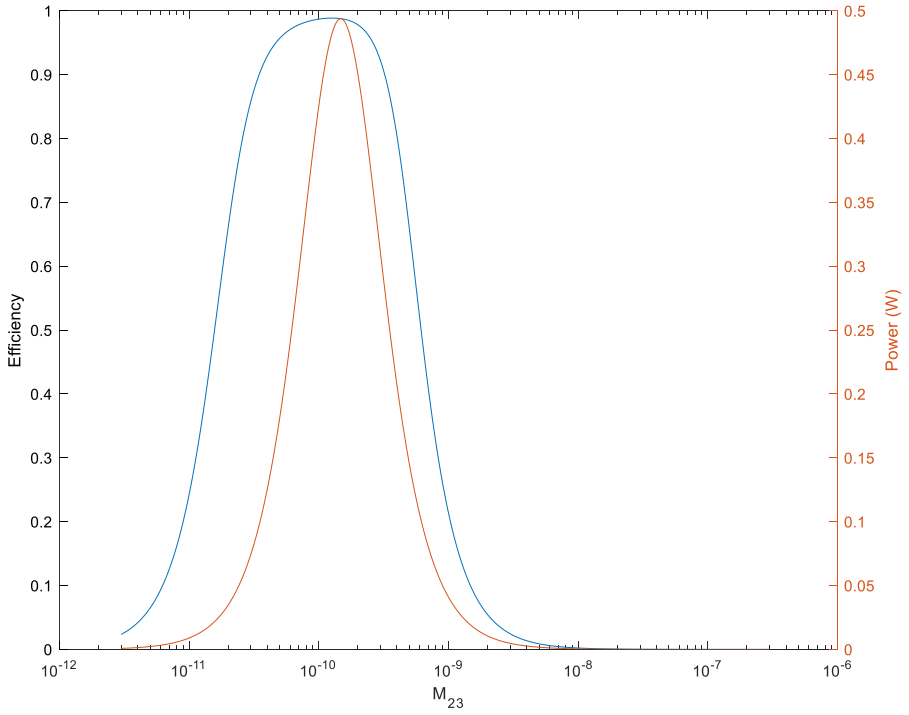

Figure 5.1.3: The Power Transfer Efficiency and Transmitted Power as a Function of M_{23} ($X_1 = 5$)

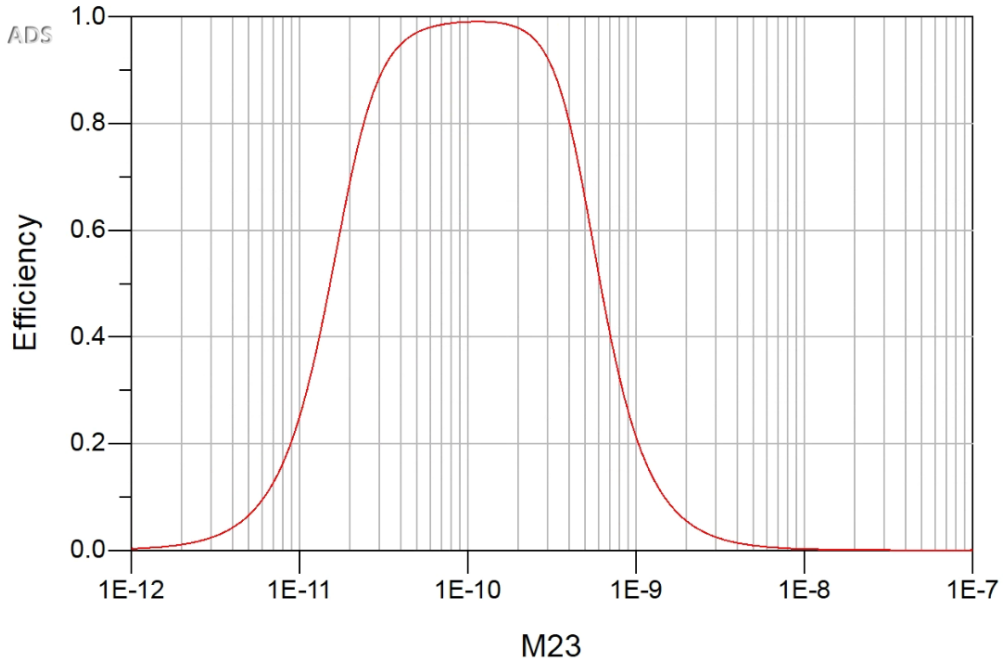

Figure 5.1.4: The Power Transfer Efficiency as a Function of M_{23} Simulated using ADS ($X_1 = 5$)

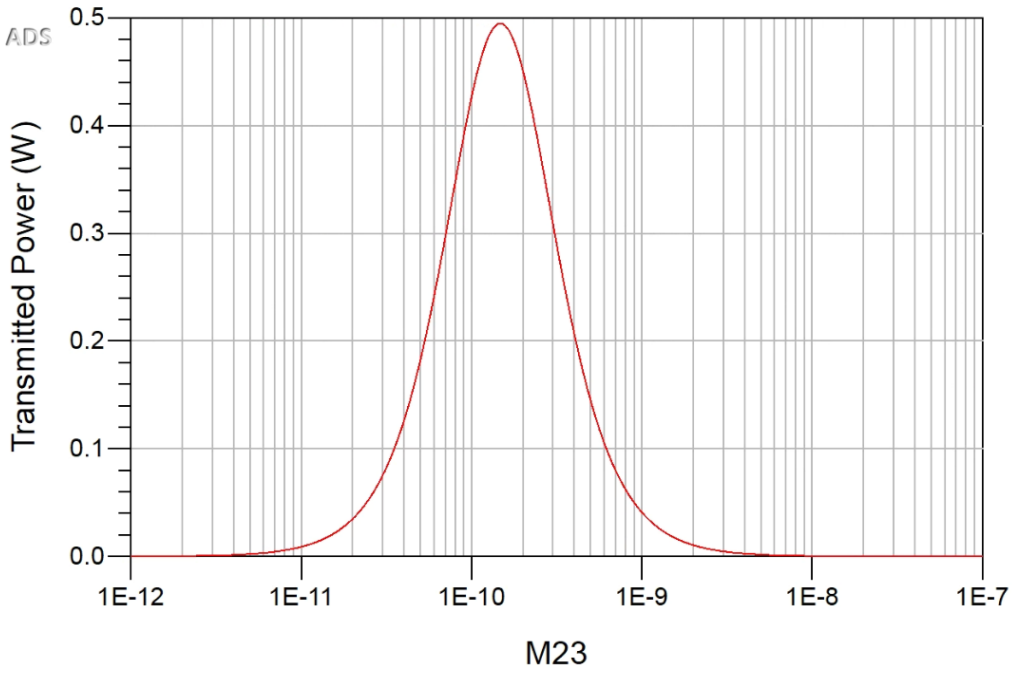

Figure 5.1.5: The Transmitted Power as a Function of M_{23} Simulated using ADS ($X_1 = 5$)

The filter parameters for this system were selected such that the passband began at a separation distance of 30 cm and ended at a distance of 1 m. This corresponds to M_{23} values of 2.6872×10^{-10} and 1.9456×10^{-11}, respectively. Examination of Figures 5.1.3 and 5.1.4 indicates that these parameters were met. The filter performance is slightly skewed when examined in relation to physical distance. This is the result of the non-linear relationship between distance and the M_{23} magnetic coupling term, as shown in Figure 5.1.6.

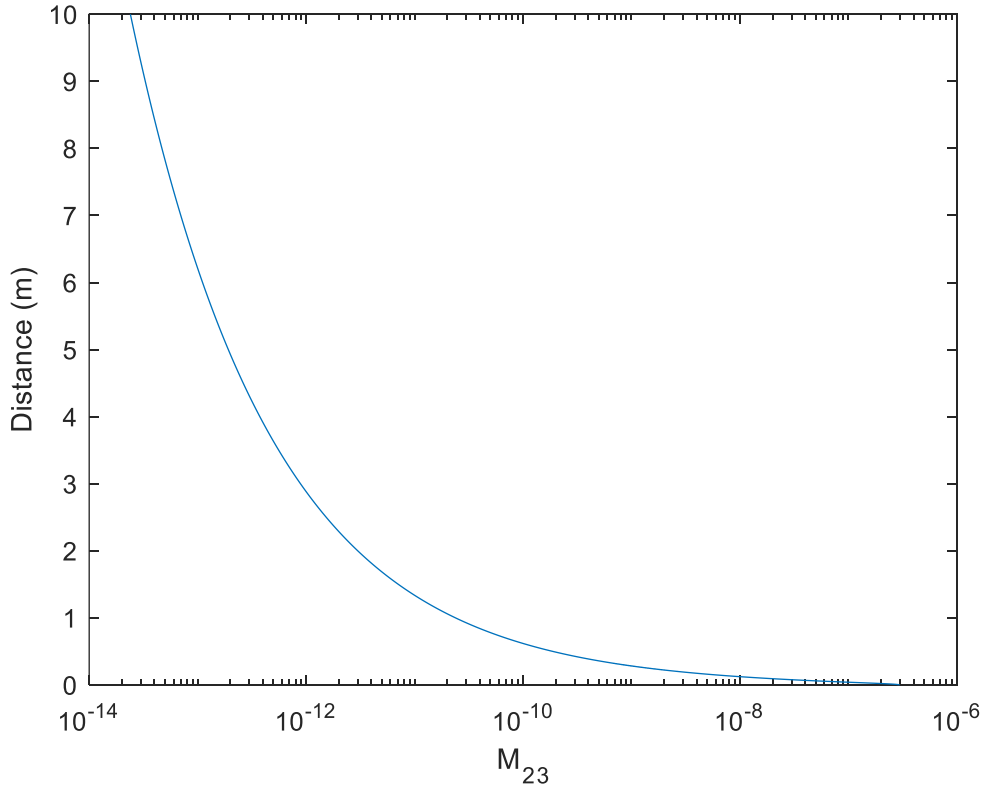

Figure 5.1.6: The Relationship Between M_{23} and Distance

Given the nature of the relationship between the two terms shown in Figure 5.1.6, changes in distances over one meter will have a much smaller effect on the magnitude of M_{23}. This causes the skewing effect on the right-hand side of Figure 5.1.2.

Next, the simulation will be repeated using the same set of coils. However, in this simulation X_1 will be set to 0.05 instead of 5. The rest of the terms from Table 5.1.2 will remain constant. The results of the general solution are shown in Table 5.1.8, and the reactive components to be added to the coils are listed in Table 5.1.9. Values for subsequent tests are also included in these tables. The power transfer efficiency and transferred power as a function of distance are shown in Figure 5.1.7.

Table 5.1.5: The Calculated Impedance Components

X_1	0.05	0.5	50
R_1	0.005	0.05	5
R_2	8.4162×10^{-2}	8.4162×10^{-3}	8.4162×10^{-5}
R_3	2.4006×10^{-10}	2.4006×10^{-9}	2.4006×10^{-7}
X_2	8.4453×10^{-1}	8.4453×10^{-2}	8.4453×10^{-4}
X_3	6.3135×10^{-4}	1.9959×10^{-3}	1.987×10^{-2}
X_4	3.9178×10^{-4}	1.2389×10^{4}	1.2379×10^{3}

Table 5.1.6: The Added Reactive Components

X_1	0.05	0.5	50
Component Added (Coil One)	Capacitor, 7.4115 nF	Capacitor, 8.6390 nF	Inductor, 1.0982 μH
Component Added (Coil Two)	Capacitor, 1.8053nF	Capacitor, 1.7056 nF	Capacitor, 1.6953 nF
Component Added (Coil Three)	Capacitor, 1.6953 nF	Capacitor, 1.6954 nF	Capacitor, 1.6976 nF
Component Added (Coil Four)	Inductor, 919.60 μH	Inductor, 290.75 μH	Inductor, 28.983 nF

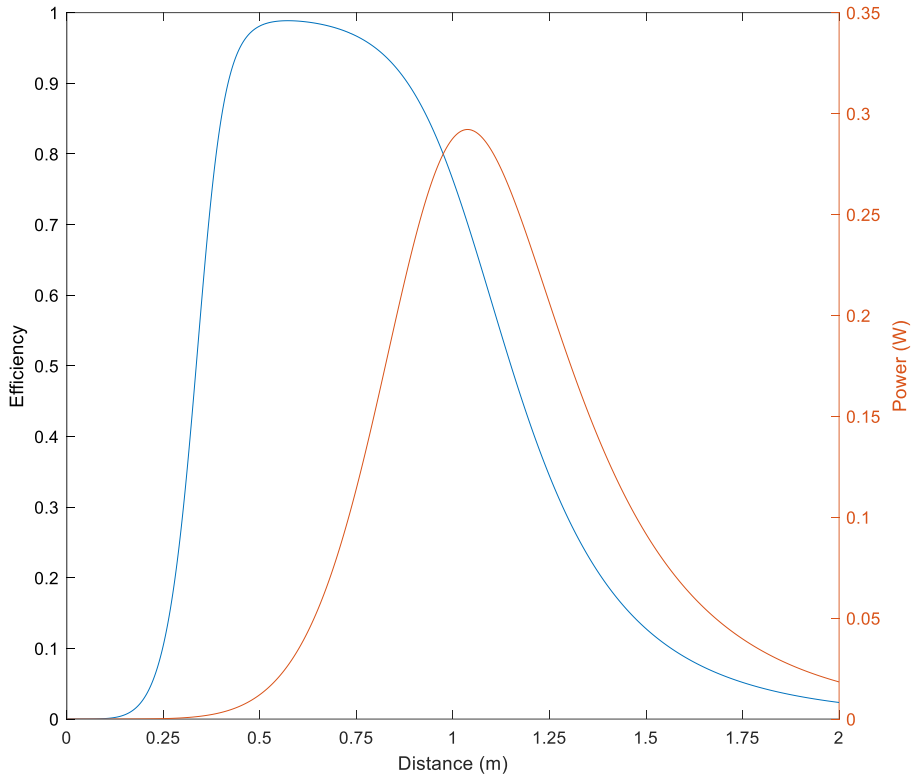

Figure 5.1.7: The Power Transfer Efficiency and Transmitted Power as a Function of Distance (X_1 = 0.05)

The transfer efficiency curve depicted in Figure 5.1.7 has not significantly changed from the curve shown in Figure 5.1.2. This points to the success of the general solution – Given an acceptable input, the solution will output impedance parameters which achieve the desired transfer function. However, the transmitted power curve has been altered by the new X_1 parameter. The maximum transmitted power now occurs at a distance of 1.04 m, as opposed to the previous configuration which peaked at a distance of 0.55 m. The magnitude of the transmitted power curve has also decreased from 0.49 W to 0.29 W.

The results of additional tests of the solution at $X_1 = 0.5$ and $X_1 = 50$ are shown in Figures 5.1.8 and 5.1.9, respectively. A plot of the maximum transmitted power and the range at which it occurs as a function of X_1 is shown in Figure 5.1.10.

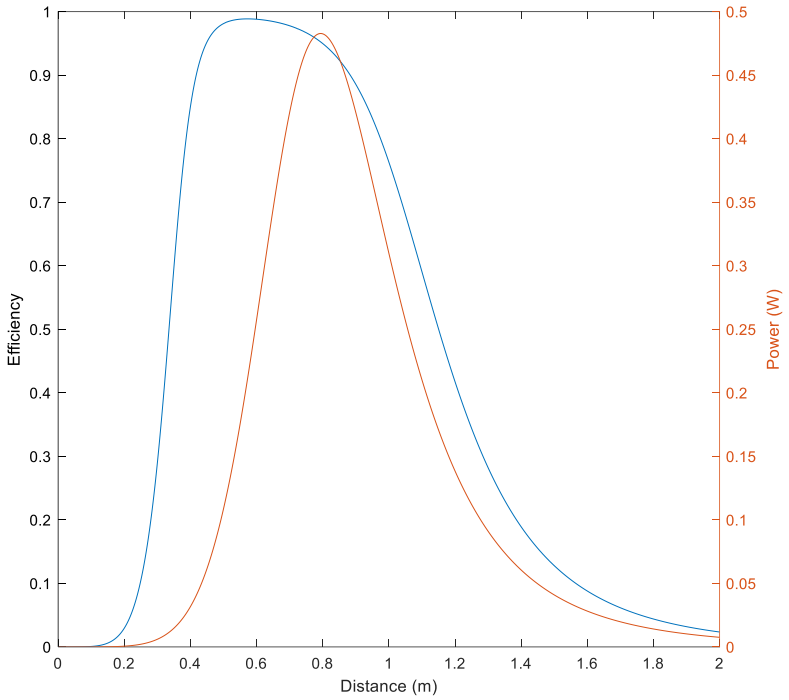

Figure 5.1.8: The Power Transfer Efficiency and Transmitted Power as a Function of Distance ($X_1 = 0.5$)

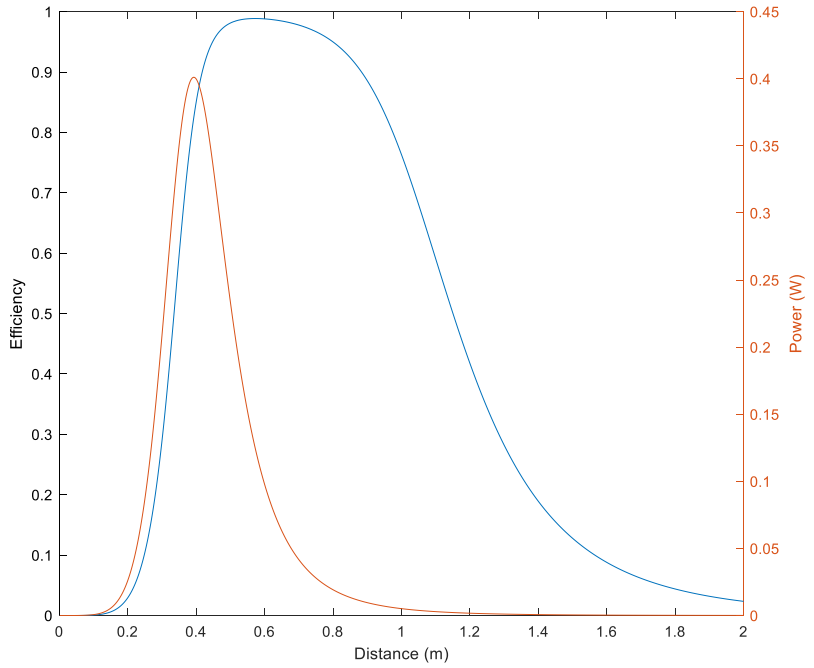

Figure 5.1.9: The Power Transfer Efficiency and Transmitted Power as a Function of Distance (X_1 = 50)

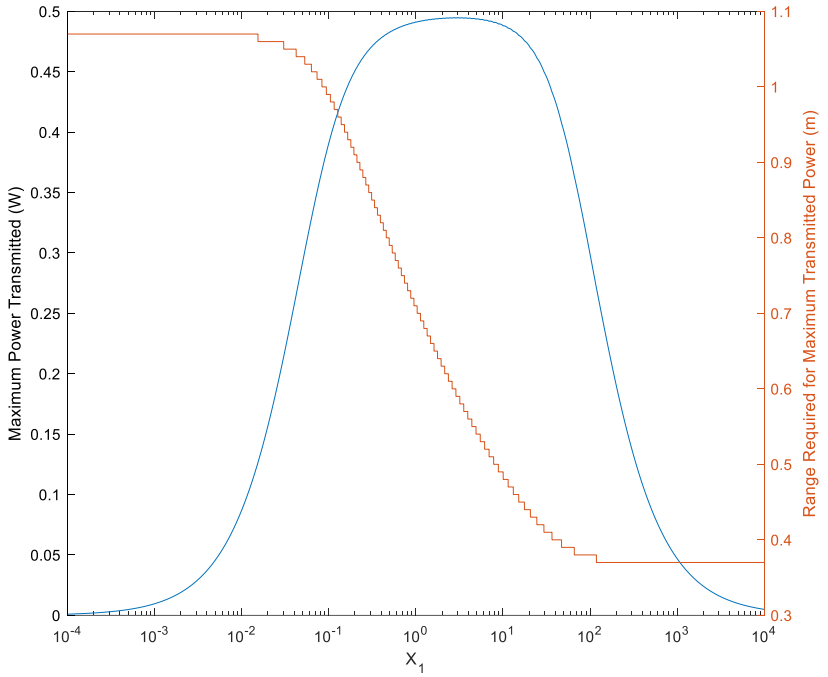

Figure 5.1.10: The Maximum Transmitted Power and Associated Range as a Function of X_1

Based on Figure 5.1.10, the general solution is capable of tuning the range of peak transmitted power via the value of X_1. Smaller values of X_1 increase the range of the peak and larger values of X_1 lead to smaller ranges. There are two drawbacks to this capability. First, the amount of power transmitted is decreased when $1 \geq X_1 \geq 10$. Second, even though the peak power transmission range changes, the efficiency curve does not. This means that additional input power may be needed to receive decreasing amounts of power.

General plots of the power transfer efficiency and the transmitted power over a range of values of X_1 and distance are shown in Figure 5.1.11 and 5.1.12.

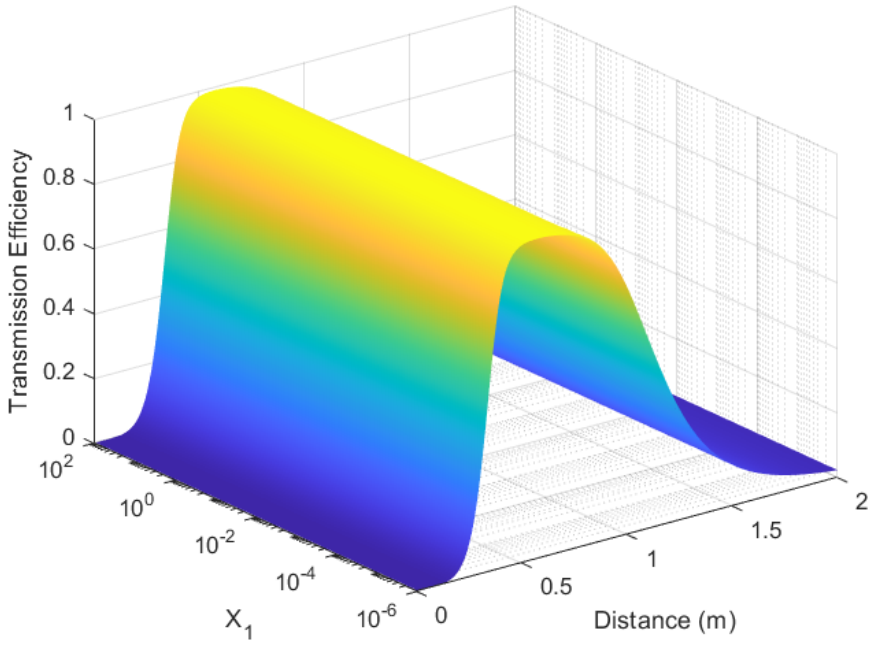

Figure 5.1.11: The Power Transfer Efficiency as a Function of X_1 and Transmission Distance

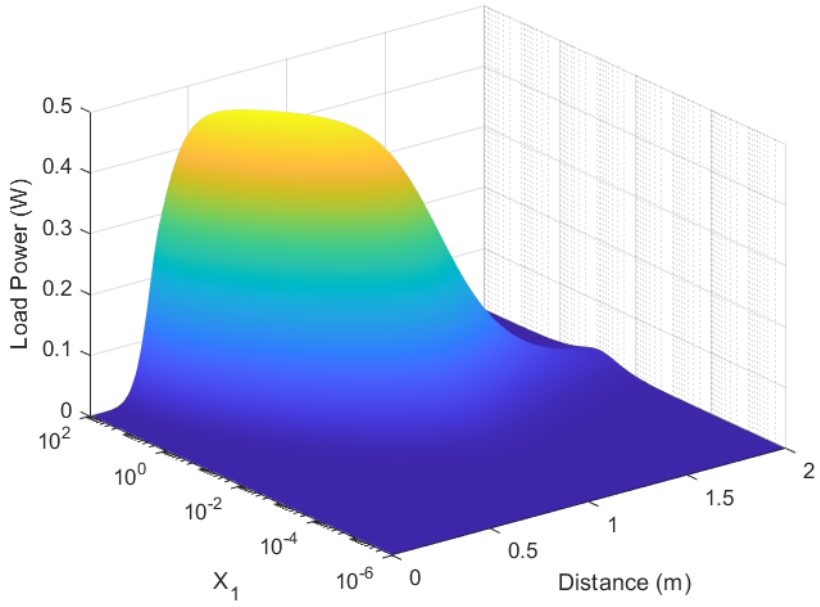

Figure 5.1.12: The Transmitted Power as a Function of X_1 and Transmission Distance

At this stage, the modified general solution should be considered.

5.2 Simulations of the Modified General Solution

The modified general solution uses the same base parameters as the standard general solution. As such, Table 5.1.2 contains all of the inputs used for this solution. Table 5.2.1 contains the impedance components required for the modified general solution, and Table 5.2.2 contains the values of the reactive components which were added to the simulated coils.

Table 5.2.1: The Impedance Components for the Modified General Solution

Parameter	Value
R_1	5
R_2	4.5761×10^{-8}
R_3	2.9520×10^{-8}
X_2	4.5761×10^{-7}
X_3	6.3×10^{-3}
X_4	3.9175×10^{3}

Table 5.2.2: The Reactive Components to be Used

Parameter	Value
Inductor (Coil One)	41.849 nH
Capacitor (Coil Two)	1.6952 nF
Capacitor (Coil Three)	1.6960 nF
Inductor (Coil Four)	91.884 μH

These components were added to the system and then simulated in Matlab and ADS. The Matlab solutions are shown in terms of distance in Figure 5.2.1 and in terms of M_{23} in Figure 5.2.2. The ADS solutions are shown in Figures 5.2.3 and 5.2.4.

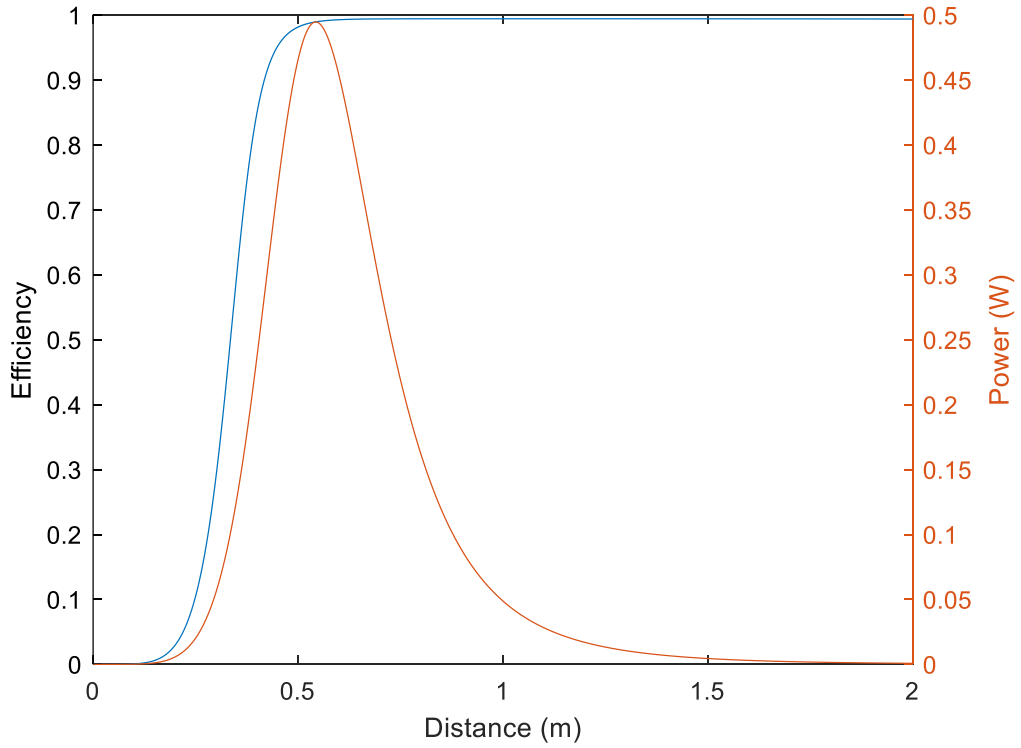

Figure 5.2.1: The Power Transfer Efficiency and Transmitted Power as a Function of Distance

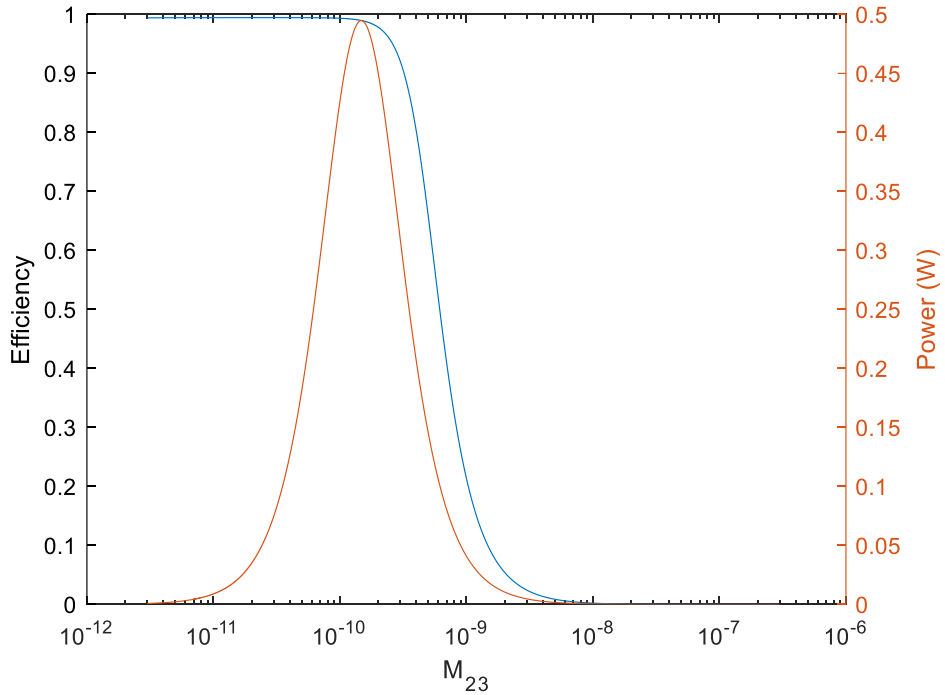

Figure 5.2.2: The Power Transfer Efficiency and Transmitted Power as a Function of M_{23}

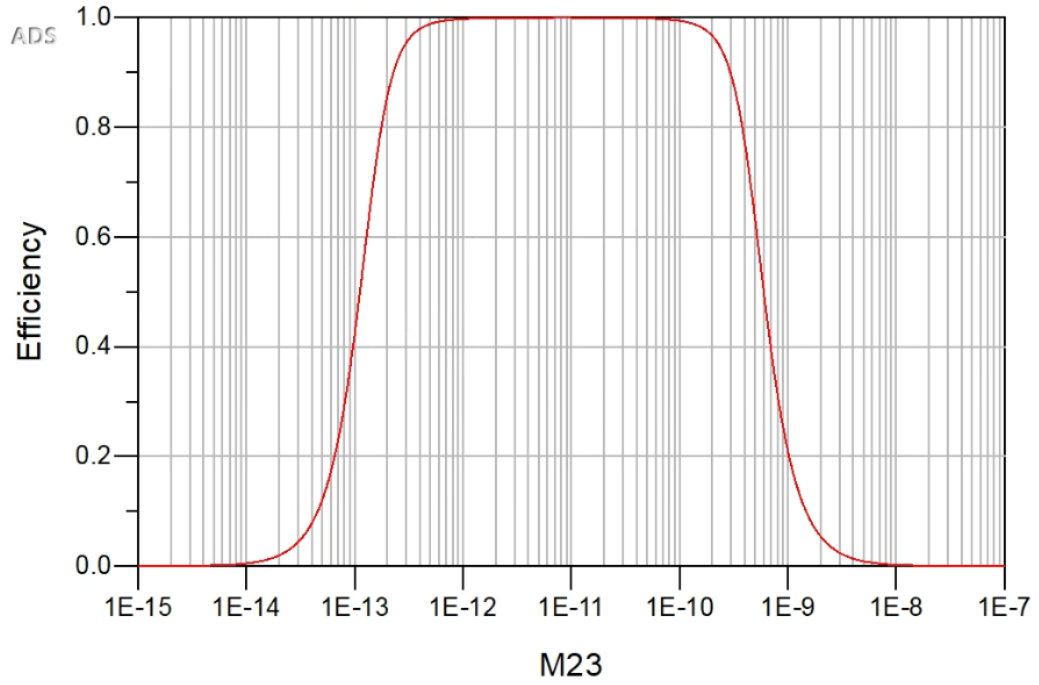

Figure 5.2.3: The Power Transfer Efficiency as a Function of M_{23}, Simulated using ADS

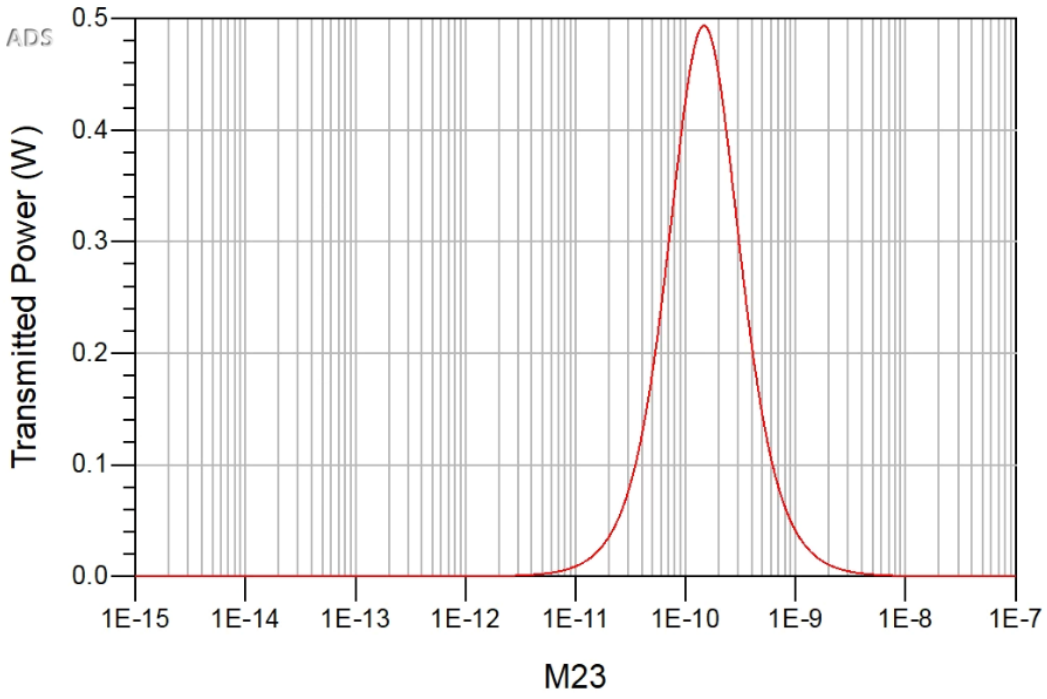

Figure 5.2.4: The Transmitted Power as a Function of M_{23}, Simulated using ADS

The key difference between the general solution and the modified general solution appears in the efficiency curve. While the general solution sees the efficiency curve peak around 50 cm and then slowly drop off, the modified solution maintains high efficiency to distances of 2 m and beyond. The curve shown in Figure 5.2.5 is taken from the same simulation as the previous images. In this case, however, the simulation is conducted out to a range of 10 m.

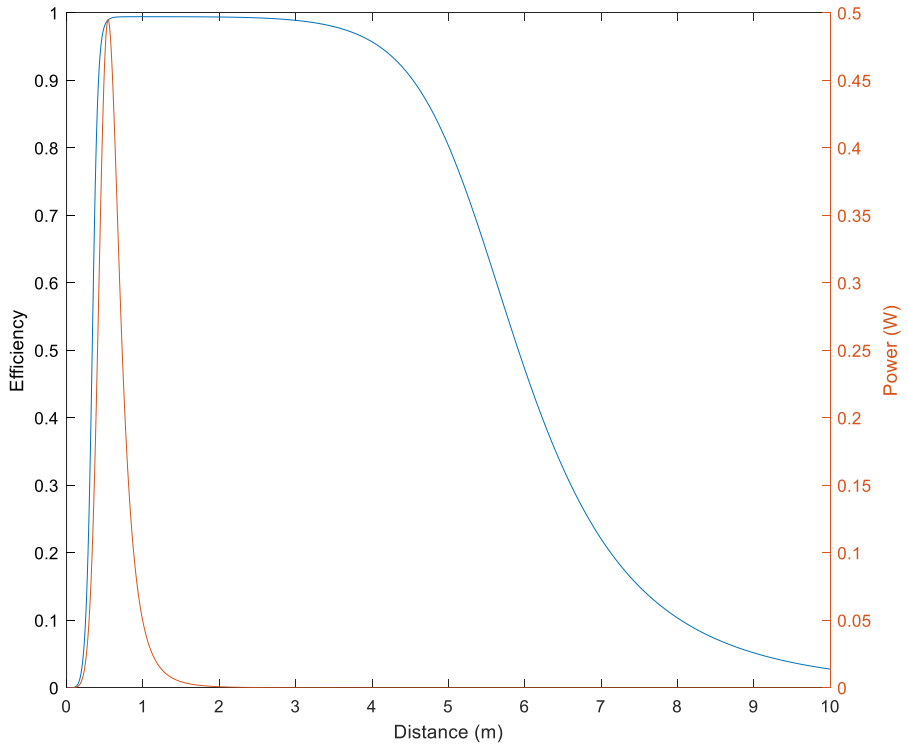

Figure 5.2.5: The Power Transfer Efficiency and Transmitted Power as a Function of Distance Modified Solution, $X_1 = 5$ over a range from 0 to 10 m

Based on the efficiency curve shown in Figure 5.2.5, transfer efficiencies of 90% or greater can be maintained at distances ranging from 41 cm to 4.5 m. This is an improvement over the previous general solution.

Next, the simulation will be repeated for different values of X_1. Table 5.2.3 lists all of the impedance components used, and Table 5.2.4 lists the values of the reactive components added. R_4 was held at 0.01 for each of these tests.

Table 5.2.3: The Impedance Components Needed

X_1 Chosen	0.5	0.05	0.005
R_1	$5.0\text{x}10^{-2}$	$5\text{x}10^{-3}$	$5\text{x}10^{-4}$
R_2	$4.5674\text{x}10^{-8}$	$4.5649\text{x}10^{-8}$	$4.5642\text{x}10^{-8}$
R_3	$2.9520\text{x}10^{-9}$	$2.9520\text{x}10^{-10}$	$2.9520\text{x}10^{-11}$
X_2	$4.5674\text{x}10^{-7}$	$4.5649\text{x}10^{-7}$	$4.5641\text{x}10^{-7}$
X_3	$2.0\text{x}10^{-3}$	$6.3135\text{x}10^{-4}$	$1.9967\text{x}10^{-4}$
X_4	$1.2389\text{x}10^{4}$	$3.9178\text{x}10^{4}$	$1.2389\text{x}10^{5}$

Table 5.2.4: The Reactive Components Added

X_1 Chosen	0.5	0.05	0.005
Coil 1	Capacitor, 8.6390 nF	Capacitor, 7.4115 nF	Capacitor, 7.3077 nF
Coil 2	Capacitor, 1.6952 nF	Capacitor, 1.6952 nF	Capacitor, 1.6952 nF
Coil 3	Capacitor, 1.6954 nF	Capacitor, 1.6953 nF	Capacitor, 1.6952 nF
Coil 4	Inductor, 290.75 μH	Inductor, 919.6 μH	Inductor, 2.9089 mH

Figures 5.2.6, 5.2.7 and 5.2.8 show the results of the revised solution for X_1 = 0.5, 0.05, and 0.005, respectively.

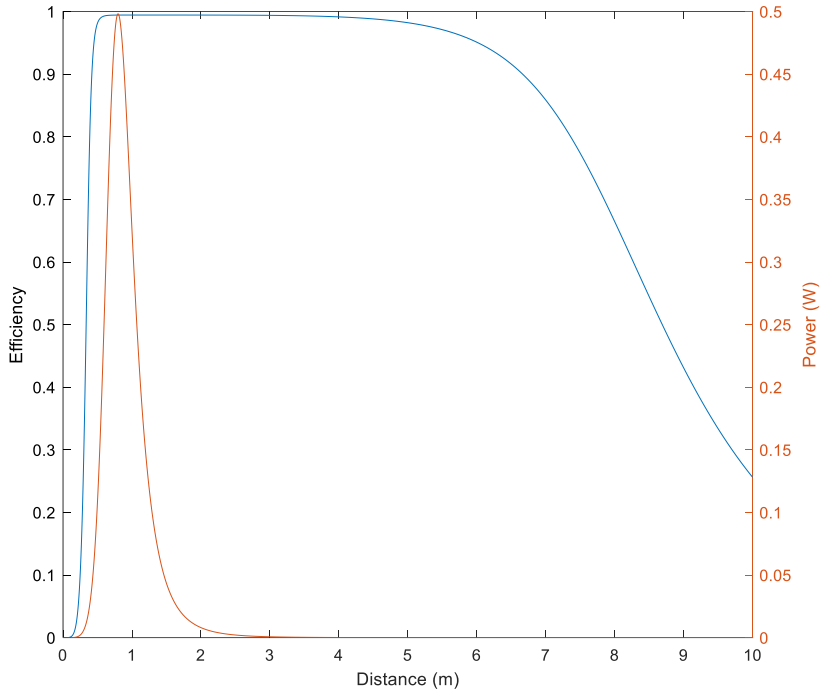

Figure 5.2.6: The Power Transfer Efficiency and Transmitted Power as a Function of Distance, Modified Solution, $X_1 = 0.5$ over a range from 0 to 10 m

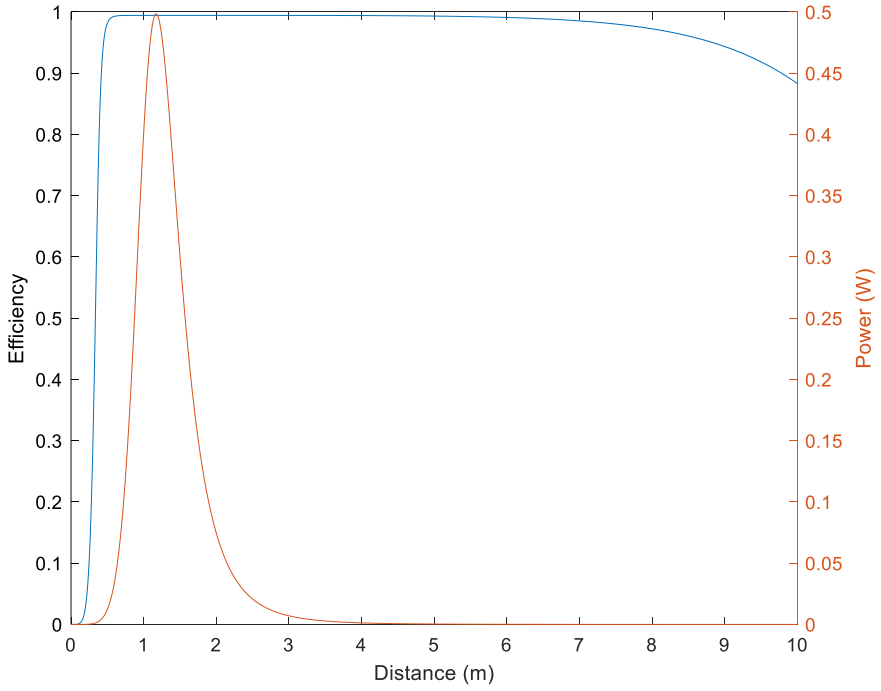

Figure 5.2.7: The Power Transfer Efficiency and Transmitted Power as a Function of Distance Modified Solution, $X_1 = 0.05$ over a range from 0 to 10 m

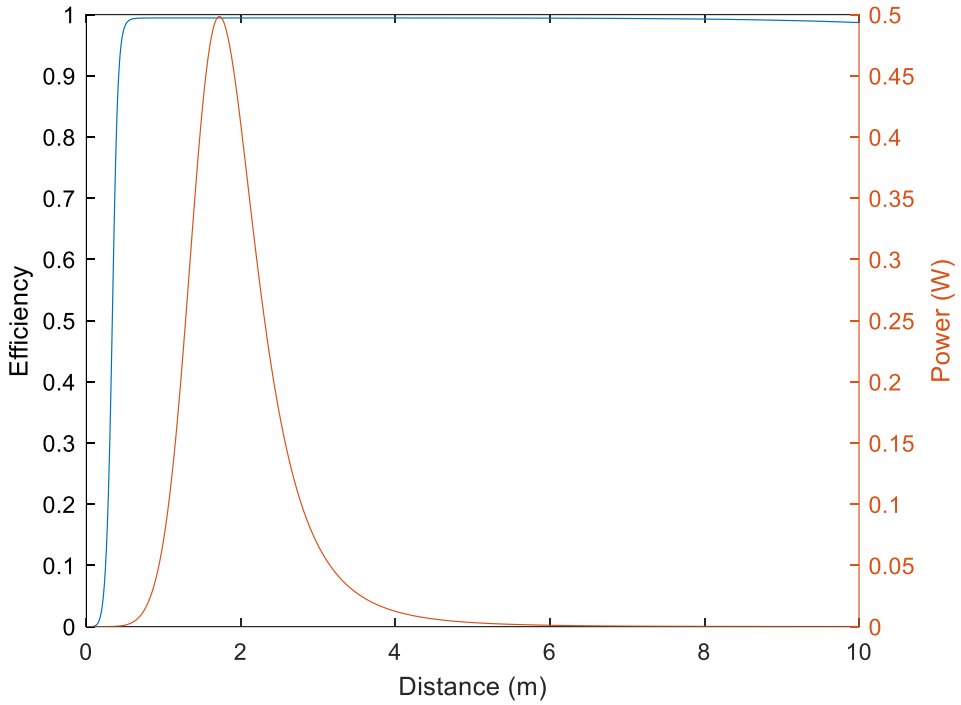

Figure 5.2.8: The Power Transfer Efficiency and Transmitted Power as a Function of Distance Modified Solution, $X_1 = 0.005$ over a range from 0 to 10 m

Based on Figure 5.2.5 through 5.2.8 as X_1 is lowered the distance at which the most power is transmitted increases. However, unlike the general solution, the amount of power transmitted does not change. Figure 5.2.9 shows a plot of the peak power transmitted and the range of peak transmission as a function of X_1 for the modified solution.

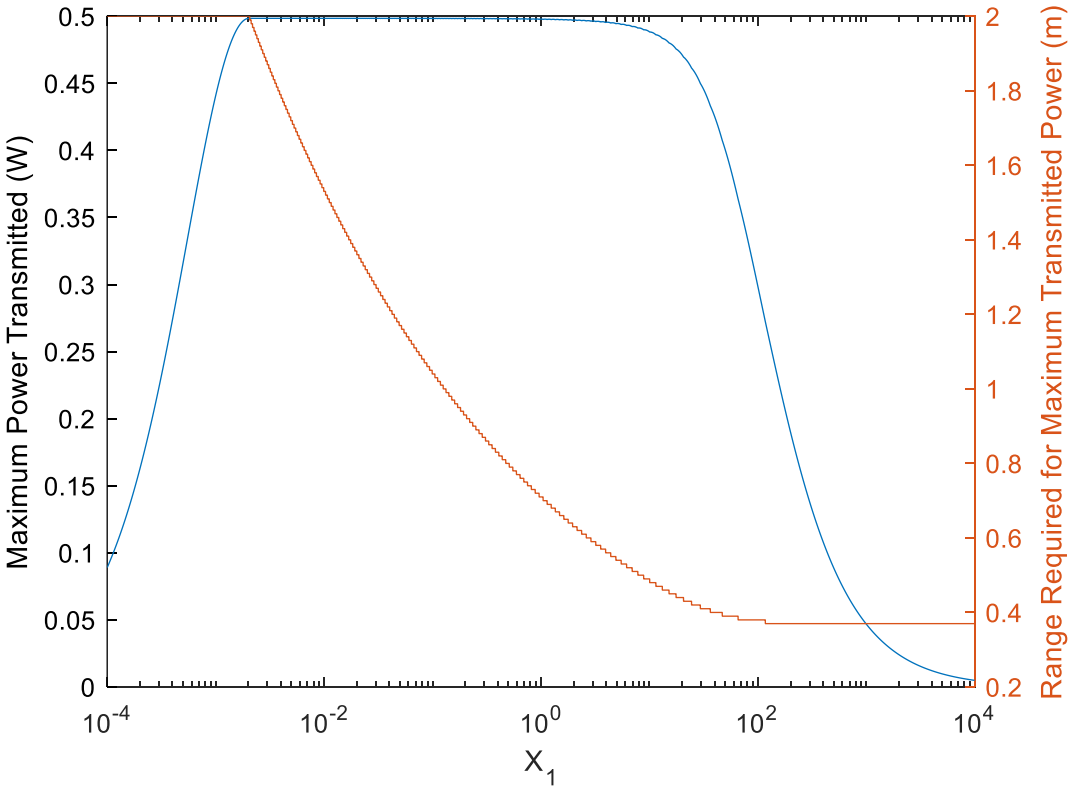

Figure 5.2.9: The Maximum Power Transmitted and Range of Maximum Transmitted Power as a Function of X_1 (Modified Solution)

Based on Figure 5.2.9, the revised solution is capable of maintaining the maximum achievable transmitted power over a range of X_1 values beginning at $1.8 * 10^{-3}$ and continuing up until 2. This corresponds to a physical distance ranging from 2 m down to 40 cm. This is a major improvement over the general solution as it allows a complete user control over the power transmission characteristics of their system.

Furthermore, this system was simulated using a source voltage of 10 V. Referring back to equation 3.1.8 for the load power of an MCRWPT system it should be noted that the load power is proportional to the square of the source voltage. If the source voltage were to be increased, this would greatly improve the power transmitted. For example, consider a source voltage of 120 V, which is the commercial voltage available. Our source voltage has increased by a factor of

twelve, so our load power will increase by a factor of 144 to 72 watts. There are some obvious limitations to this concept. Larger voltages will create larger currents, which the transmission coils will likely not be capable of handling. Larger voltages will also create larger magnetic fields which may be harmful to people or equipment. Regardless of these limitations, the fact remains that it appears to be possible to tune the range and magnitude of power transmitted without observing major losses at the circuit level.

Finally, general plots of the power transfer efficiency and transmitted power as a function of X_1 and distance for the modified solution are shown in Figures 5.2.10 and 5.2.11.

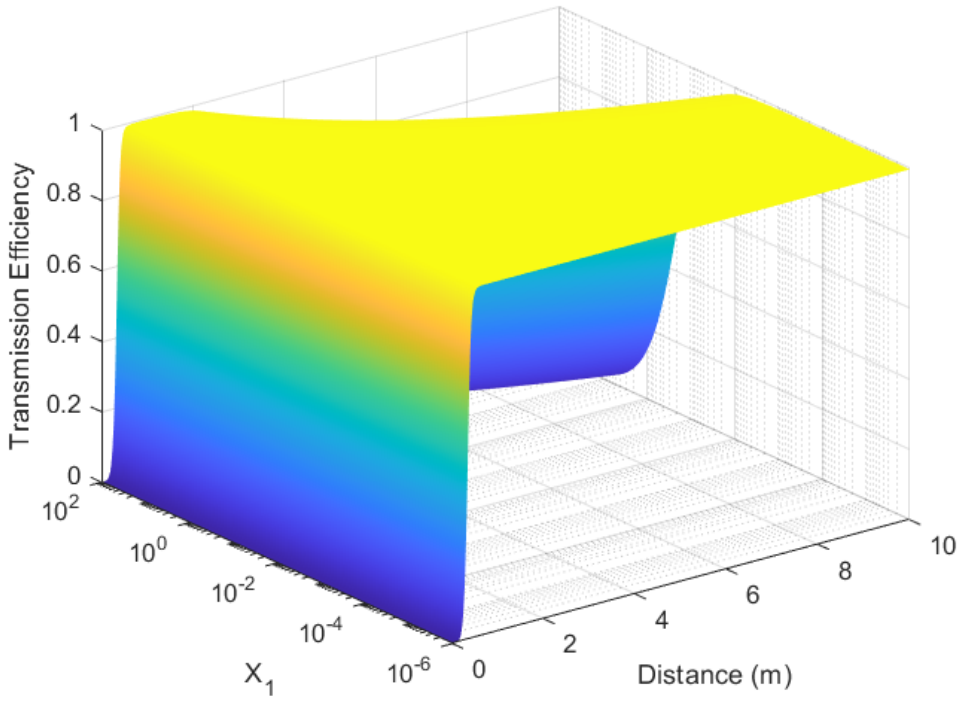

Figure 5.2.10: The Power Transfer Efficiency as a Function of X_1 and Distance for the Modified Solution

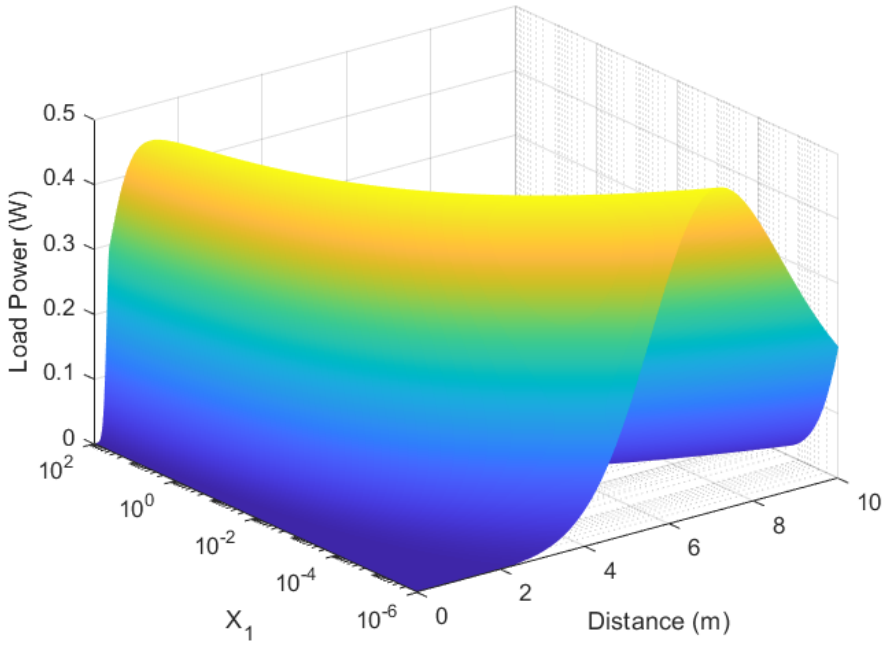

Figure 5.2.11: The Transmitted Power as a Function of X_1 and Distance for the Modified Solution

Figure 5.2.10 clearly shows that smaller values of X_1 will yield a longer range of high-efficiency transmission. Mathematically this trend appears to continue on well beyond the range of X_1 and distance values simulated here. However, it is important to note that R_1 is constrained to being at least ten times smaller in magnitude than X_1. Thus, there is a physical limit to the maximum capabilities of this design scheme.

5.3 Summary of Findings and Discussion

The simulations described in this section have clearly shown that designs generated using the solutions developed in Section Four are capable of meeting the requirements set out by the filter parameters. In addition, the modified general solution is also capable of maintaining a high power output over a wide range of distances when X_1 is modified accordingly. This means the performance of an MCRWPT system can be successfully predicted and controlled via a filter transfer function. This provides system designers with additional control over their designs.

Chapter 6 Conclusion

As a whole, it has been shown that the MCRWPT theory is compatible with the existing filter theory. The range of filters which can be implemented may be limited due to a lack of poles and zeros, although sufficient terms are available to produce a bandpass filter's transfer function. Bridging or mapping functions were also identified which allow for filter transfer functions to be realized using coil impedance terms.

Two solutions to the bridging functions have been presented. The first was obtained through a rigorous derivation of the bridging functions. This solution reproduces the desired transfer function characteristics in the power transfer efficiency at a wide range of values for X_1. It was found that the magnitude of the load power was dependant on the value of X_1, and that the distance at which the maximum load power was observed could be controlled by the value of X_1 as well. In general, smaller values of X_1 were associated with maximum load power occurring at greater distances, and larger values of X_1 were associated with maximum load power occurring at shorter distances. Unfortunately, it was also found that there was an ideal value for X_1 which maximized the amount of load power observed. Whenever the value of X_1 was displaced from this value, the maximum load power which was observed decreased.

The second general solution shared many of the properties associated with the first solution. However, unlike the first solution, the power transfer efficiency curve was affected by the value of X_1, and smaller values of X_1 were shown to increase the range of high-efficiency energy transfer. This solution was also capable of shifting the distance at which maximum load power was observed without decreasing the magnitude of load power observed.

Overall, filter theory was proved to be a viable technique for the design of MCRWPT systems.

6.1 Recommendations for Future Work

The work shown here illustrates that filter transfer functions can be successfully applied to a theoretical MCRWPT system design. However, physical tests of this concept were not possible due to ongoing COVD-19 related lab closures. As such, these design techniques should be tested on physical systems to determine if their theoretical performance can be realized in an actual system.

In addition, while two potential solutions are shown, they are by no means the only possible solutions. As such, further work should be invested in identifying alternate solutions to bridging equations that result in physically realizable systems.

Alternatively, load power could be maintained through the arraying of multiple systems configured for maximum load power at different coil separations. This is a concept that should be investigated further.

Filter theory presents a convenient methodology for the manipulation and control of the MCRWPT efficiency function. Given the success which has already been observed, it is worth considering whether these techniques could be applied to other areas of MCRWPT theory, such as load power. If this were to be successful, then an engineer might be able to design a wideband system which would have uniform performance over a range of coil separations without resorting to an arrayed approach.

References

[1] International Data Corporation, "The Growth in Connected IoT Devices Is Expected to Generate 79.4ZB of Data in 2025, According to a New IDC Forecast," *IDC Media Center,* 2019. [Online] Available: https://www.idc.com [Accessed: July 31, 2020].

[2] Statista, "IoT: number of connected devices worldwide 2012-2025," *Statista Research Department,* 2016. [Online] Available: https://www.statista.com/statistics/ [Accessed July 31, 2020].

[3] S. Y. R. Hui, W. Zhong, and C. K. Lee, "A critical review of recent progress in midrange wireless power transfer," Power Electronics, IEEE Transactions on, vol. 29, no. 9, pp. 4500-4511, 2014.

[4] A. Karalis, J. D. Joannopoulos, and M. Soljačić, "Efficient wireless non-radiative midrange energy transfer," Annals of Physics, vol. 323, no. 1, pp. 34-48, 1 2008.

[5] L. Gao, X. Fan, C. Wang, Y. Tan and X. Zhang, "Coil Design of EVs Wireless Charging System Based on MCR-WPT," *2018 11th International Symposium on Computational Intelligence and Design (ISCID)*, Hangzhou, China, 2018, pp. 169-172, doi: 10.1109/ISCID.2018.10140.

[6] T. Campi, S. Cruciani, M. Feliziani and A. Hirata, "Wireless power transfer system applied to an active implantable medical device," *2014 IEEE Wireless Power Transfer Conference*, Jeju, 2014, pp. 134-137, doi: 10.1109/WPT.2014.6839612.

[7] A. M. Jawad, H. M. Jawad, R. Nordin, S. K. Gharghan, N. F. Abdullah and M. J. Abu-Alshaeer, "Wireless Power Transfer With Magnetic Resonator Coupling and Sleep/Active Strategy for a Drone Charging Station in Smart Agriculture," in *IEEE Access*, vol. 7, pp. 139839-139851, 2019, doi: 10.1109/ACCESS.2019.2943120.

[8] F. Jolani, "Wireless Power Transfer Via Magnetic Resonant Coupling," Ph.D thesis, Dalhousie University, Halifax, NS, 2015.

[9] Z. Wang, X. Wang and B. Zhang, "A magnetic coupled resonance WPT system design method of double-end impedance converter networks with Class-E amplifier," *IECON 2015 - 41st Annual Conference of the IEEE Industrial Electronics Society*, Yokohama, 2015, pp. 003093-003098, doi: 10.1109/IECON.2015.7392575.

[10] X. Zhang, L. Gao, C. Wang, Z. Wang and X. Fan, "Design and Simulation Analysis on the Transmitter/Receiver of MCR-WPT," *2018 11th International Symposium on Computational Intelligence and Design (ISCID)*, Hangzhou, China, 2018, pp. 157-160, doi: 10.1109/ISCID.2018.10137.

[11] Otto J. Zobel, "Theory and design of uniform and composite electric wave-filters," *The Bell System Technical Journal*, 2(1):1-46, January 1923

[12] S. Butterworth, "On the Theory of Filter Amplifiers," *Experimental Wireless & the Wireless Engineer*, vol. 7, no. 85, Oct., pp. 536-541 1930.

[13] G. A. Campbell, "Electric Wave-Filter," U. S. Patent 1,227,113, 15 Jul, 1915

[14] N. Telsa, "System of Transmission of Electrical Energy," U.S. Patent 645,576A, 20 Mar, 1900

[15] W. C. Brown, "The history of wireless power transmission," Solar Energy, vol. 56, no. 1, pp. 3-21, 1996.

[16] W. C. Brown, "Experiments involving a microwave beam to power and position a helicopter," Aerospace and Electronic Systems, IEEE Transactions on, vol. AES-5, no. 5, pp. 692-702, 1969.

[17] M. Galizzi, M. Caldara, V. Re and A. Vitali, "A novel Qi-standard compliant full-bridge wireless power charger for low power devices," *2013 IEEE Wireless Power Transfer (WPT)*, Perugia, 2013, pp. 44-47, doi: 10.1109/WPT.2013.6556877.

[18] F. Liu, Y. Yang, Z. Ding, X. Chen and R. M. Kennel, "A Multifrequency Superposition Methodology to Achieve High Efficiency and Targeted Power Distribution for a Multiload MCR WPT System," in *IEEE Transactions on Power Electronics*, vol. 33, no. 10, pp. 9005-9016, Oct. 2018, doi: 10.1109/TPEL.2017.2784566.

[19] F. Liu, Z. Ding, X. Fu and R. M. Kennel, "Parametric Optimization of a Three-Phase MCR WPT System With Cylinder-Shaped Coils Oriented by Soft-Switching Range and Stable Output Power," in *IEEE Transactions on Power Electronics*, vol. 35, no. 1, pp. 1036-1044, Jan. 2020, doi: 10.1109/TPEL.2019.2914154.

[20] S. Raju, R. Wu, M. Chan, and C. P. Yue, "Modeling of mutual coupling between planar inductors in wireless power applications," Power Electronics, IEEE Transactions on, vol. 29, no. 1, pp. 481-490, 2014.

[21] D. Song, F. Shi, S. Dai and L. Liu, "Design and analysis of a wireless power transmission system with magnetic coupling resonance in the weak-coupling region," in *Chinese Journal of Electrical Engineering*, vol. 5, no. 4, pp. 51-60, Dec. 2019, doi: 10.23919/CJEE.2019.000027.

[22] C. Xiao, D. Cheng and K. Wei, "An LCC-C Compensated Wireless Charging System for Implantable Cardiac Pacemakers: Theory, Experiment, and Safety Evaluation," in *IEEE Transactions on Power Electronics*, vol. 33, no. 6, pp. 4894-4905, June 2018, doi: 10.1109/TPEL.2017.2735441.

[23] L. Shuguang, Y. Zhenxing and L. Wenbin, "Design and Simulation of Coupling Coil for EV's Wireless Charging System," *2018 IEEE International Conference on Electronics and Communication Engineering (ICECE)*, Xi'an, China, 2018, pp. 115-119, doi: 10.1109/ICECOME.2018.8644810.

[24] J. Shin *et al*., "Design of buried power line for roadway-powered electric vehicle system," *2013 IEEE Wireless Power Transfer (WPT)*, Perugia, 2013, pp. 56-57, doi: 10.1109/WPT.2013.6556880.

[25] W. Ying, L. Weiguo, H. Hongyun, L. Zongjian, X. Yang and L. Da, "Research on Contactless Power Supply of High Speed Maglev Train Based on MCR-WPT," *2019 14th IEEE Conference on Industrial Electronics and Applications (ICIEA)*, Xi'an, China, 2019, pp. 2297-2302, doi: 10.1109/ICIEA.2019.8834278.

[26] M. Molefi, E. D. Markus and A. Abu-Mahfouz, "Wireless Power Transfer for LoRa Low-Power wide-area Networks (LPWANs)," *2019 Southern African Universities Power Engineering Conference/Robotics and Mechatronics/Pattern Recognition Association of South Africa (SAUPEC/RobMech/PRASA)*, Bloemfontein, South Africa, 2019, pp. 105-110, doi: 10.1109/RoboMech.2019.8704805.

[27] C. Qi, T. Lin, Z. Wang, D. Li and T. Sun, "Research on metal object detection of MCR-WPT system that allows transmisson coils to be misaligned," *IECON 2019 - 45th Annual Conference of the IEEE Industrial Electronics Society*, Lisbon, Portugal, 2019, pp. 4642-4647, doi: 10.1109/IECON.2019.8927616.

[28] J. Park, Y. Tak, Y. Kim, Y. Kim, and S. Nam, "Investigation of adaptive matching methods for near-field wireless power transfer," Antennas and Propagation, IEEE Transactions on, vol. 59, no. 5, pp. 1769-1773, 2011.

[29] K. E. Koh, T. C. Beh, T. Imura, and Y. Hori, "Impedance matching and power division using impedance inverter for wireless power transfer via magnetic resonant coupling," Industry Applications, IEEE Transactions on, vol. 50, no. 3, pp. 2061-2070, 2014.

[30] F. Liu, Y. Yang, Z. Ding, X. Chen and R. M. Kennel, "Eliminating cross interference between multiple receivers to achieve targeted power distribution for a multifrequency multi-load MCR WPT system," in *IET Power Electronics*, vol. 11, no. 8, pp. 1321-1328, 10 7 2018, doi: 10.1049/iet-pel.2017.0770.

[31] W. Peng and Z. Chen, "Enhanced Planar Wireless Power Transfer Systems with Ferrite Material," *2018 IEEE Wireless Power Transfer Conference (WPTC)*, Montreal, QC, Canada, 2018, pp. 1-4, doi: 10.1109/WPT.2018.8639455.

[32] Y. Nishizawa, Y. Narusue and Y. Kawahara, "Enhancing the quality factor of thin film printed coils for efficient wireless power transfer," *2018 IEEE Radio and Wireless Symposium (RWS)*, Anaheim, CA, 2018, pp. 25-27, doi: 10.1109/RWS.2018.8304936.

[33] H Baher, *Signal Processing and Integrated Circuits.* West Sussex, United Kingdom: John Wiley & Sons Ltd, 2012.

APPENDIX A: MATLAB Code Developed for this Thesis

```
%MCRWPT_FILTERTHEORY.m
%Aleksander Jack, Last Updated August 30th, 2020
%General purpose Diagnostic/Figure Generation Code
%
%In the interests of improving readability and reducing the risk of
%improperly configuring/typing variables, X 1-4 and R 1-4 are
%substituted for A-H.
%R1 = A, R2 = C, R3 = E, R4 = G
%X1 = B, X2 = D, X3 = F, X4 = H
%
% General Purpose code used in the process of developing the thesis
% Used to generate most if not all plots taken from MATLAB
%

clear all

%Preset all physical constants
uo = 4e-7*pi;
eo = 8.854e-12;
f = 6.87e6; %Corresponds to an ISM band
w= 2*pi*f;
sigma_trace = 5.96e7;
e_air = 1.0006*eo;
e_sub = 4.7*eo;
delta = 1/sqrt(pi*f*uo*sigma_trace);
Beta = 0; %Parameters described in [8] for PSC M calculations
Sigma = 0; %Parameters described in [8] for PSC M calculations

%Load/Source Configuration
RLd = 50;
Rx = 1/RLd; %Used to simplify the algebra
Rs = 50;
Vs = 10;
%10V is used as a sample value. Vs has no impact on the efficiency formula
%and only acts as a uniform scaling factor on the amount of power received

%Configure range of coil separations to be used
D23Count = 5000;
D23Min = 0.01;
D23Max = 10;
D23_Range = linspace(D23Min,D23Max,D23Count);

%Configure range of X1 values to be used
BMin = 1e-6;
BMax = 100;
BCount = 500;
B = logspace(log10(BMin),log10(BMax),BCount);

%Note: Either D23Count or BCount may be set to 1 to run a one-dimensional
%sweep if desired.

% Coil Data Structure
% 1 = Ro
% 2 = Ri
```

```
% 3 = Wr
% 4 = S
% 5 = T
% 6 = N
% 7 = G (Gap in coil due to connections)

% Using 0.0347mm as trace depth
% All Measurements in Meters (Base SI)

%Two coil forms possible
SmallYellowTx = [0.03,0.026,0.004,0,0.0000347,1,0.003;0.05,0.034,0.006,0.004,0.0000347,2,0.01];
SmallYellowRx = [0.05,0.034,0.006,0.004,0.0000347,2,0.01;0.03,0.026,0.004,0,0.0000347,1,0.003];
LargeYellowTx = [0.1,0.068,0.012,0.012,0.0000347,2,0.003;0.0515,0.043,0.0085,0,0.0000347,1,0.03];
LargeYellowRx = [0.0515,0.043,0.0085,0,0.0000347,1,0.03;0.1,0.068,0.012,0.012,0.0000347,2,0.003];

%Determines which coils will be used to send/receive
coil = [SmallYellowTx;SmallYellowRx];

%Calculation of Coil Parameters, per [8]
Phi = (coil(:,1)-coil(:,2))./(coil(:,1)+coil(:,2));
Ravg = (coil(:,1)+coil(:,2))/2;

L = 1.27*uo*coil(:,6).^2.*Ravg/2.*(log(2.07./Phi)+0.18*Phi+0.13*Phi.^2);
L1=L(1);
L2=L(2);
L3=L(3);
L4=L(4);

lg = 4*(2*coil(:,1)-coil(:,3).*coil(:,6)).*(coil(:,6)-1)-4*coil(:,4).*coil(:,6).*(coil(:,6)+1);
lt = 4*(coil(:,2).*coil(:,6)+coil(:,6).^2.*coil(:,3)+coil(:,6).*(coil(:,6)-1).*coil(:,4))-coil(:,6).*coil(:,7)+(coil(:,6)-
1).*sqrt((coil(:,3)+coil(:,4)).^2+coil(:,7).^2);

C = (0.9*e_air+0.1*e_sub)*eo*coil(:,5)./coil(:,4).*lg;
Rdc = lt./(sigma_trace*coil(:,5).*coil(:,3));

Rskin = Rdc.*(coil(:,5)./(delta*(1-exp(-coil(:,5)/delta)).*(1+coil(:,5)./coil(:,3))));
Rp = Rdc*(Beta*f+Sigma*f^2);
Rtot = Rskin + Rp;
R1=Rtot(1);
R2=Rtot(2);
R3=Rtot(3);
R4=Rtot(4);

%Calculate M23 Values for chosen coils/distance configuration, per [8]
count1 = 1;
for D23 = D23_Range
   M=zeros(4);
for a=1:1:4
   for b=1:1:4
      if a>=b
         continue
      end
      if ((a==1)&&(b==2))||((a==3)&&(b==4))
         z = 0;
      else
         z = D23;
```

```
        end
        for na=1:1:coil(a,6)
            for nb=1:1:coil(b,6)
                ai = coil(a,1)-(coil(a,6)-1)*(coil(a,3)+coil(a,4))-coil(a,3)/2;
                bj = coil(b,1)-(coil(b,6)-1)*(coil(b,3)+coil(b,4))-coil(b,3)/2;
                yij=2*ai*bj/(ai^2+bj^2+z^2);
                M(a,b) = M(a,b)+uo*pi*ai^2*bj^2/(2*(ai^2+bj^2+z^2)^1.5)*(1+15/32*yij^2+315/1024*yij^4);
            end
        end
    end
end

M = M*(4/pi)^2;
M12 = M(1,2);
M23_Range(count1) = M(2,3);
M34 = M(3,4);
count1 = count1+1;
end

%Filter cutoff values for small coils
wl = 7.2213e-20; %30cm
wh = 3.7854e-22; %100cm

%1.6205e-16; %10cm
%1.3356e-19; %40cm

neta = 3.0424; %Chosen per [33]

Top = i*neta^2*wl/(w^6*M12^2*M34^2*Rx);

%Terms to control the ratio between desired and undesired terms in the
%bridging functions
gamma2 = 1;
gamma1 = 1;
gamma0 = 1;

%Intial Configuration of Impedance Variables
A = B/(10*gamma2);
C = 1E-10*ones(1,BCount);
E = A;
G = 0.01*ones(1,BCount);
H = sqrt(w^2*M12^2*M34^2*Rx./(neta*wl*B)-G.^2*Rx^2-2*G*Rx-1)/Rx;
D = 1E-10*ones(1,BCount);

for iteration =1:1:15
    %Two Solutions have been identified. Only one can be run at a time.

    %Modified Solution
    F = -((wl.*neta.^2 + wh)./(10.*gamma1) - H.*Rx.*neta.^2.*wl - (2.*A.*D.*neta.^2.*wl)./(M12.^2.*w.^2) +
(2.*B.*C.*G.*Rx.*neta.^2.*wl)./(M12.^2.*w.^2) + (2.*B.*D.*H.*Rx.*neta.^2.*wl)./(M12.^2.*w.^2) -
(2.*A.*D.*E.*neta.^2.*wl)./(M12.^2.*M34.^2.*Rx.*w.^4) -
(2.*A.*C.*E.*H.*neta.^2.*wl)./(M12.^2.*M34.^2.*w.^4) +
(2.*B.*C.*E.*G.*neta.^2.*wl)./(M12.^2.*M34.^2.*w.^4) -
(2.*A.*D.*E.*G.*neta.^2.*wl)./(M12.^2.*M34.^2.*w.^4) +
(2.*B.*D.*E.*H.*neta.^2.*wl)./(M12.^2.*M34.^2.*w.^4) +
(2.*B.*C.*E.*G.^2.*Rx.*neta.^2.*wl)./(M12.^2.*M34.^2.*w.^4) +
```

```
(2.*B.*C.*E.*H.^2.*Rx.*neta.^2.*wl)./(M12.^2.*M34.^2.*w.^4))./((2.*G.*neta.^2.*wl)./(M34.^2.*w.^2) +
(neta.^2.*wl)./(M34.^2.*Rx.*w.^2) + (G.^2.*Rx.*neta.^2.*wl)./(M34.^2.*w.^2) +
(H.^2.*Rx.*neta.^2.*wl)./(M34.^2.*w.^2) - (2.*A.*C.*neta.^2.*wl)./(M12.^2.*M34.^2.*Rx.*w.^4) -
(2.*A.*C.*G.*neta.^2.*wl)./(M12.^2.*M34.^2.*w.^4) + (2.*B.*C.*H.*neta.^2.*wl)./(M12.^2.*M34.^2.*w.^4) +
(2.*A.*D.*H.*neta.^2.*wl)./(M12.^2.*M34.^2.*w.^4) - (2.*B.*D.*G.*neta.^2.*wl)./(M12.^2.*M34.^2.*w.^4) -
(2.*B.*D.*G.^2.*Rx.*neta.^2.*wl)./(M12.^2.*M34.^2.*w.^4) -
(2.*B.*D.*H.^2.*Rx.*neta.^2.*wl)./(M12.^2.*M34.^2.*w.^4));

   E = -(G.*Rx.*neta.^2.*wl - wh + (2.*B.*D.*neta.^2.*wl)./(M12.^2.*w.^2) +
(2.*A.*C.*G.*Rx.*neta.^2.*wl)./(M12.^2.*w.^2) + (2.*A.*D.*H.*Rx.*neta.^2.*wl)./(M12.^2.*w.^2) +
(2.*B.*C.*F.*neta.^2.*wl)./(M12.^2.*M34.^2.*Rx.*w.^4) +
(2.*A.*C.*F.*H.*neta.^2.*wl)./(M12.^2.*M34.^2.*w.^4) +
(2.*B.*C.*F.*G.*neta.^2.*wl)./(M12.^2.*M34.^2.*w.^4) -
(2.*A.*D.*F.*G.*neta.^2.*wl)./(M12.^2.*M34.^2.*w.^4) -
(2.*B.*D.*F.*H.*neta.^2.*wl)./(M12.^2.*M34.^2.*w.^4) -
(2.*A.*D.*F.*G.^2.*Rx.*neta.^2.*wl)./(M12.^2.*M34.^2.*w.^4) -
(2.*A.*D.*F.*H.^2.*Rx.*neta.^2.*wl)./(M12.^2.*M34.^2.*w.^4))./((2.*G.*neta.^2.*wl)./(M34.^2.*w.^2) +
(neta.^2.*wl)./(M34.^2.*Rx.*w.^2) + (G.^2.*Rx.*neta.^2.*wl)./(M34.^2.*w.^2) +
(H.^2.*Rx.*neta.^2.*wl)./(M34.^2.*w.^2) + (2.*B.*D.*neta.^2.*wl)./(M12.^2.*M34.^2.*Rx.*w.^4) +
(2.*A.*C.*G.*neta.^2.*wl)./(M12.^2.*M34.^2.*w.^4) + (2.*B.*C.*H.*neta.^2.*wl)./(M12.^2.*M34.^2.*w.^4) +
(2.*A.*D.*H.*neta.^2.*wl)./(M12.^2.*M34.^2.*w.^4) + (2.*B.*D.*G.*neta.^2.*wl)./(M12.^2.*M34.^2.*w.^4) +
(2.*A.*C.*G.^2.*Rx.*neta.^2.*wl)./(M12.^2.*M34.^2.*w.^4) +
(2.*A.*C.*H.^2.*Rx.*neta.^2.*wl)./(M12.^2.*M34.^2.*w.^4));

   sqbrak = (E.^2+F.^2)./(neta*wl*B)+w^2*M34^2*Rx;
   Csqrt = sqrt(w^4*M12^4+B*wh*w^4./(25*gamma2*gamma0*neta*sqbrak)-B.^2.*D.^2/(25*gamma2^2));
   C = (-w^2*M12^2+Csqrt)./(B/(5*gamma2));
   Dsqrt = sqrt(w^4*M12^4-4*B*wh*w^4./(neta*sqbrak)-4*B.^2.*C.^2);
   D = (-w^2*M12^2+Dsqrt)./(-2*B);

   %General Solution
   % F = -((wl.*neta.^2 + wh)./(10.*chi1) - H.*Rx.*neta.^2.*wl + (2.*B.*C.*neta.^2.*wl)./(M12.^2.*w.^2) +
(2.*B.*C.*G.*Rx.*neta.^2.*wl)./(M12.^2.*w.^2) + (2.*B.*D.*H.*Rx.*neta.^2.*wl)./(M12.^2.*w.^2) +
(2.*B.*C.*E.*neta.^2.*wl)./(M12.^2.*M34.^2.*Rx.*w.^4) +
(4.*B.*C.*E.*G.*neta.^2.*wl)./(M12.^2.*M34.^2.*w.^4) +
(2.*B.*C.*E.*G.^2.*Rx.*neta.^2.*wl)./(M12.^2.*M34.^2.*w.^4) +
(2.*B.*C.*E.*H.^2.*Rx.*neta.^2.*wl)./(M12.^2.*M34.^2.*w.^4))./((2.*G.*neta.^2.*wl)./(M34.^2.*w.^2) +
(neta.^2.*wl)./(M34.^2.*Rx.*w.^2) + (G.^2.*Rx.*neta.^2.*wl)./(M34.^2.*w.^2) +
(H.^2.*Rx.*neta.^2.*wl)./(M34.^2.*w.^2) - (2.*B.*D.*neta.^2.*wl)./(M12.^2.*M34.^2.*Rx.*w.^4) -
(4.*B.*D.*G.*neta.^2.*wl)./(M12.^2.*M34.^2.*w.^4) -
(2.*B.*D.*G.^2.*Rx.*neta.^2.*wl)./(M12.^2.*M34.^2.*w.^4) -
(2.*B.*D.*H.^2.*Rx.*neta.^2.*wl)./(M12.^2.*M34.^2.*w.^4));

   % E = (wh - G.*Rx.*neta.^2.*wl - (2.*A.*C.*neta.^2.*wl)./(M12.^2.*w.^2) -
(2.*A.*C.*G.*Rx.*neta.^2.*wl)./(M12.^2.*w.^2) - (2.*A.*D.*H.*Rx.*neta.^2.*wl)./(M12.^2.*w.^2) +
(2.*A.*D.*F.*neta.^2.*wl)./(M12.^2.*M34.^2.*Rx.*w.^4) +
(4.*A.*D.*F.*G.*neta.^2.*wl)./(M12.^2.*M34.^2.*w.^4) +
(2.*A.*D.*F.*G.^2.*Rx.*neta.^2.*wl)./(M12.^2.*M34.^2.*w.^4) +
(2.*A.*D.*F.*H.^2.*Rx.*neta.^2.*wl)./(M12.^2.*M34.^2.*w.^4))./((2.*G.*neta.^2.*wl)./(M34.^2.*w.^2) +
(neta.^2.*wl)./(M34.^2.*Rx.*w.^2) + (G.^2.*Rx.*neta.^2.*wl)./(M34.^2.*w.^2) +
(H.^2.*Rx.*neta.^2.*wl)./(M34.^2.*w.^2) + (2.*A.*C.*neta.^2.*wl)./(M12.^2.*M34.^2.*Rx.*w.^4) +
(4.*A.*C.*G.*neta.^2.*wl)./(M12.^2.*M34.^2.*w.^4) +
(2.*A.*C.*G.^2.*Rx.*neta.^2.*wl)./(M12.^2.*M34.^2.*w.^4) +
(2.*A.*C.*H.^2.*Rx.*neta.^2.*wl)./(M12.^2.*M34.^2.*w.^4));
```

```
    % C = -(E.^2.*M12.^2.*w.^2 - (((E.^2.*G.^2.*Rx.^2 + 2.*E.^2.*G.*Rx + E.^2.*H.^2.*Rx.^2 + E.^2 +
2.*E.*G.*M34.^2.*Rx.^2.*w.^2 + 2.*E.*M34.^2.*Rx.*w.^2 + F.^2.*G.^2.*Rx.^2 + 2.*F.^2.*G.*Rx +
F.^2.*H.^2.*Rx.^2 + F.^2 - 2.*F.*H.*M34.^2.*Rx.^2.*w.^2 + M34.^4.*Rx.^2.*w.^4).*(-
20.*chi0.*A.^2.*D.^2.*E.^2.*G.^2.*Rx.^2 - 40.*chi0.*A.^2.*D.^2.*E.^2.*G.*Rx -
20.*chi0.*A.^2.*D.^2.*E.^2.*H.^2.*Rx.^2 - 20.*chi0.*A.^2.*D.^2.*E.^2 -
40.*chi0.*A.^2.*D.^2.*E.*G.*M34.^2.*Rx.^2.*w.^2 - 40.*chi0.*A.^2.*D.^2.*E.*M34.^2.*Rx.*w.^2 -
20.*chi0.*A.^2.*D.^2.*F.^2.*G.^2.*Rx.^2 - 40.*chi0.*A.^2.*D.^2.*F.^2.*G.*Rx -
20.*chi0.*A.^2.*D.^2.*F.^2.*H.^2.*Rx.^2 - 20.*chi0.*A.^2.*D.^2.*F.^2 +
40.*chi0.*A.^2.*D.^2.*F.*H.*M34.^2.*Rx.^2.*w.^2 - 20.*chi0.*A.^2.*D.^2.*M34.^4.*Rx.^2.*w.^4 +
2.*wh.*A.*M12.^2.*M34.^2.*Rx.*w.^6 + 5.*chi0.*E.^2.*G.^2.*M12.^4.*Rx.^2.*w.^4 +
10.*chi0.*E.^2.*G.*M12.^4.*Rx.*w.^4 + 5.*chi0.*E.^2.*H.^2.*M12.^4.*Rx.^2.*w.^4 +
5.*chi0.*E.^2.*M12.^4.*w.^4 + 10.*chi0.*E.*G.*M12.^4.*M34.^2.*Rx.^2.*w.^6 +
10.*chi0.*E.*M12.^4.*M34.^2.*Rx.*w.^6 + 5.*chi0.*F.^2.*G.^2.*M12.^4.*Rx.^2.*w.^4 +
10.*chi0.*F.^2.*G.*M12.^4.*Rx.*w.^4 + 5.*chi0.*F.^2.*H.^2.*M12.^4.*Rx.^2.*w.^4 +
5.*chi0.*F.^2.*M12.^4.*w.^4 - 10.*chi0.*F.*H.*M12.^4.*M34.^2.*Rx.^2.*w.^6 +
5.*chi0.*M12.^4.*M34.^4.*Rx.^2.*w.^8))./(5.*chi0)).^(1./2) + F.^2.*M12.^2.*w.^2 +
M12.^2.*M34.^4.*Rx.^2.*w.^6 + 2.*E.^2.*G.*M12.^2.*Rx.*w.^2 + 2.*F.^2.*G.*M12.^2.*Rx.*w.^2 +
2.*E.*M12.^2.*M34.^2.*Rx.*w.^4 + E.^2.*G.^2.*M12.^2.*Rx.^2.*w.^2 + F.^2.*G.^2.*M12.^2.*Rx.^2.*w.^2 +
E.^2.*H.^2.*M12.^2.*Rx.^2.*w.^2 + F.^2.*H.^2.*M12.^2.*Rx.^2.*w.^2 +
2.*E.*G.*M12.^2.*M34.^2.*Rx.^2.*w.^4 - 2.*F.*H.*M12.^2.*M34.^2.*Rx.^2.*w.^4)./(2.*(A.*E.^2.*G.^2.*Rx.^2
+ 2.*A.*E.^2.*G.*Rx + A.*E.^2.*H.^2.*Rx.^2 + A.*E.^2 + 2.*A.*E.*G.*M34.^2.*Rx.^2.*w.^2 +
2.*A.*E.*M34.^2.*Rx.*w.^2 + A.*F.^2.*G.^2.*Rx.^2 + 2.*A.*F.^2.*G.*Rx + A.*F.^2.*H.^2.*Rx.^2 + A.*F.^2 -
2.*A.*F.*H.*M34.^2.*Rx.^2.*w.^2 + A.*M34.^4.*Rx.^2.*w.^4));

    % D = (E.^2.*M12.^2.*w.^2 - (-(E.^2.*G.^2.*Rx.^2 + 2.*E.^2.*G.*Rx + E.^2.*H.^2.*Rx.^2 + E.^2 +
2.*E.*G.*M34.^2.*Rx.^2.*w.^2 + 2.*E.*M34.^2.*Rx.*w.^2 + F.^2.*G.^2.*Rx.^2 + 2.*F.^2.*G.*Rx +
F.^2.*H.^2.*Rx.^2 + F.^2 - 2.*F.*H.*M34.^2.*Rx.^2.*w.^2 +
M34.^4.*Rx.^2.*w.^4).*(4.*B.^2.*C.^2.*E.^2.*G.^2.*Rx.^2 + 8.*B.^2.*C.^2.*E.^2.*G.*Rx +
4.*B.^2.*C.^2.*E.^2.*H.^2.*Rx.^2 + 4.*B.^2.*C.^2.*E.^2 + 8.*B.^2.*C.^2.*E.*G.*M34.^2.*Rx.^2.*w.^2 +
8.*B.^2.*C.^2.*E.*M34.^2.*Rx.*w.^2 + 4.*B.^2.*C.^2.*F.^2.*G.^2.*Rx.^2 + 8.*B.^2.*C.^2.*F.^2.*G.*Rx +
4.*B.^2.*C.^2.*F.^2.*H.^2.*Rx.^2 + 4.*B.^2.*C.^2.*F.^2 - 8.*B.^2.*C.^2.*F.*H.*M34.^2.*Rx.^2.*w.^2 +
4.*B.^2.*C.^2.*M34.^4.*Rx.^2.*w.^4 + 4.*wh.*B.*M12.^2.*M34.^2.*Rx.*w.^6 -
E.^2.*G.^2.*M12.^4.*Rx.^2.*w.^4 - 2.*E.^2.*G.*M12.^4.*Rx.*w.^4 - E.^2.*H.^2.*M12.^4.*Rx.^2.*w.^4 -
E.^2.*M12.^4.*w.^4 - 2.*E.*G.*M12.^4.*M34.^2.*Rx.^2.*w.^6 - 2.*E.*M12.^4.*M34.^2.*Rx.*w.^6 -
F.^2.*G.^2.*M12.^4.*Rx.^2.*w.^4 - 2.*F.^2.*G.*M12.^4.*Rx.*w.^4 - F.^2.*H.^2.*M12.^4.*Rx.^2.*w.^4 -
F.^2.*M12.^4.*w.^4 + 2.*F.*H.*M12.^4.*M34.^2.*Rx.^2.*w.^6 - M12.^4.*M34.^4.*Rx.^2.*w.^8)).^(1./2) +
F.^2.*M12.^2.*w.^2 + M12.^2.*M34.^4.*Rx.^2.*w.^6 + 2.*E.^2.*G.*M12.^2.*Rx.*w.^2 +
2.*F.^2.*G.*M12.^2.*Rx.*w.^2 + 2.*E.*M12.^2.*M34.^2.*Rx.*w.^4 + E.^2.*G.^2.*M12.^2.*Rx.^2.*w.^2 +
F.^2.*G.^2.*M12.^2.*Rx.^2.*w.^2 + E.^2.*H.^2.*M12.^2.*Rx.^2.*w.^2 + F.^2.*H.^2.*M12.^2.*Rx.^2.*w.^2 +
2.*E.*G.*M12.^2.*M34.^2.*Rx.^2.*w.^4 - 2.*F.*H.*M12.^2.*M34.^2.*Rx.^2.*w.^4)./(2.*(B.*E.^2.*G.^2.*Rx.^2
+ 2.*B.*E.^2.*G.*Rx + B.*E.^2.*H.^2.*Rx.^2 + B.*E.^2 + 2.*B.*E.*G.*M34.^2.*Rx.^2.*w.^2 +
2.*B.*E.*M34.^2.*Rx.*w.^2 + B.*F.^2.*G.^2.*Rx.^2 + 2.*B.*F.^2.*G.*Rx + B.*F.^2.*H.^2.*Rx.^2 + B.*F.^2 -
2.*B.*F.*H.*M34.^2.*Rx.^2.*w.^2 + B.*M34.^4.*Rx.^2.*w.^4));

end

%--------------------------------------------------------------------------
%Diagnostic system.
%Allows calculated values of M4/M2/M0 to be compared to their desired
%values over the full range of X1 (B) to identify any regions where the
%desired values are not being met. Comment this section out if it is not
%being used.

%Form Resistances/Reactances into lumped impedances for coefficient calc
Z1 = A+i*B;
Z2 = C+i*D;
```

```
Z3 = E+i*F;
Z4 = G+i*H;

%Calculate all coefficients for Filter
Num = w^6*M12^2*M34^2*Rx*Top;
M4 = Z1.*w.^4.*(Z4.*Rx+1).*(conj(Z4).*Rx+1).*Top;

M2 =
Z1.*w.^2.*(Z4.*Rx+1).*conj(Z2).*(conj(Z3).*(conj(Z4).*Rx+1)+w.^2.*M34.^2.*Rx).*Top+w.^2.*(conj(Z4).*Rx+
1).*Top.*Z1.*Z2.*(Z3.*(Z4.*Rx+1)+w.^2.*M34.^2.*Rx)+w.^4.*M12.^2.*(conj(Z4).*Rx+1).*Top.*(Z3.*(Z4.*Rx+
1)+w.^2.*M34.^2.*Rx);

M0 =
(Z1.*Z2.*(Z3.*(Z4.*Rx+1)+w.^2.*M34.^2.*Rx)+w.^2.*M12.^2.*(Z3.*(Z4.*Rx+1)+w.^2.*M34.^2.*Rx)).*conj(Z2
).*(conj(Z3).*(conj(Z4).*Rx+1)+w.^2.*M34.^2.*Rx).*Top;

%Desired Values
M4_D = -neta*(1+i/(10*gamma2))*ones(1,BCount);
M2_D = (neta^2*wl+wh)*(i+1/(10*gamma1))*ones(1,BCount);
M0_D = neta*wl*wh*(1+i/(10*gamma0))*ones(1,BCount);
%--------------------------------------------------------------------------

%Preinitialize PTE variable
PTE = zeros(BCount,D23Column);

%Main two dimensional sweep
%Begin sweeping by X1 (B) value
for CountB = 1:1:BCount

   %Display current progress in % and a time stamp
   CL = clock;
   disp([CL(4) CL(5)])
   disp([CountB/BCount*100])

   %Form Resistances/Reactances into lumped impedance
   Z1 = A(CountB)+i*B(CountB);
   Z2 = C(CountB)+i*D(CountB);
   Z3 = E(CountB)+i*F(CountB);
   Z4 = G(CountB)+i*H(CountB);

   %Begin sweeping by separation range
   CountM23 = 1;
   for M23 = M23_Range

      %Solving MCRWPT Circuit Via Impedance Matrix
      Z = [Rs+Z1,-i*w*M12,0,0;-i*w*M12,Z2,-i*w*M23,0;0,-i*w*M23,Z3,-i*w*M34;0,0,-i*w*M34,Z4+RLd];
      V = [Vs,0,0,0];
      Z_ = inv(Z);

      I = V*Z_;

      %Calculate Load/Source Voltage/Power
      VIn = Vs-Rs*I(1);
      VLd = I(4)*RLd;
      PIn = VIn*conj(I(1));
      PLd(CountB,CountM23) = VLd*conj(I(4));
```

```
        %Calculate PTE via Impedance Matrix/Circuit solution
        PTE_Z(CountB,CountM23) = PLd(CountB,CountM23)/PIn;

        %Calculate PTE via Efficiency Formula
        ALPHA = Z2*(Z3*(Z4*Rx+1)+w^2*M34^2*Rx)+w^2*M23^2*(Z4*Rx+1);
        BETA = w^2*M12^2*(Z3*(Z4*Rx+1)+w^2*M34^2*Rx);
        PTE_TF(CountB,CountM23) = abs(w^6*M12^2*M23^2*M34^2*Rx/((Z1*ALPHA+BETA)*conj(ALPHA)));

        %Increment for next run
        CountM23=CountM23+1;
    end

    %Used to generate plots 5.1.10 and 5.2.9.
    [MaxPLd(CountB),PLdRange]=max(PLd(CountB,:));
    MaxPLDRange(CountB)=D23_Range(PLdRange);
end

%Generate 3Axis plot, 5.1.12 and 5.2.11
figure()
surf(D23_Range,B,abs(PLd))
set(gca,'YScale','log')
shading interp
xlabel('Distance (m)')
ylabel('X_1')
zlabel('Load Power (W)')

%Generate 3Axis plot, 5.1.11 and 5.2.10
figure()
surf(D23_Range,B,abs(PTE_Z))
set(gca,'YScale','log')
shading interp
xlabel('Distance (m)')
ylabel('X_1')
zlabel('Efficiency')

%Generate plot 5.1.10 or 5.2.9
figure()
semilogx(B,MaxPLd)
ylabel("Maximum Power Transmitted (W)")
yyaxis right
semilogx(B,MaxPLDRange)
ylabel("Range Required for Maximum Transmitted Power")
xlable("X_1")
```